

Detrital zircon geochronology of
Permian – Triassic fluvial sediments
of the Sydney Basin: Provenance
analysis and Geomorphological effects
of the Permian –Triassic Extinction

Thesis submitted in accordance with the requirements of the University of
Adelaide for an Honours Degree in Geology/Geophysics

[Michael Joshua Morton]

November 2015



THE UNIVERSITY
of ADELAIDE

**DETRITAL ZIRCON GEOCHRONOLOGY OF PERMIAN – TRIASSIC FLUVIAL
SEDIMENTS OF THE SYDNEY BASIN: PROVENANCE ANALYSIS AND
GEOMORPHOLOGICAL EFFECTS OF THE PERMIAN – TRIASSIC EXTINCTION**

DETRITAL GEOCHONOLGY ON THE P-T BOUNDARY OF THE SYDNEY BASIN

ABSTRACT

Detrital zircons from Permian and Triassic sediments of the Sydney Basin were analysed for U-Pb geochronology to determine their provenance and to evaluate potential geomorphological effects for the Permian-Triassic mass-extinction event. Five major age peaks were obtained for the zircon U-Pb age distribution diagrams:

Cryogenian (~700-620 Ma); Cambrian (~540-490 Ma); Silurian - Devonian (~440-390 Ma); Carboniferous (~360-300 Ma) and Permian - Triassic (~280-240 Ma). These age peaks reflect pulses of significant magmatism within sediment source regions. Most detrital zircons in the analysed Sydney Basin sediments are late Palaeozoic in age and are thought to be derived from the New England Fold Belt that underwent deformation during the Hunter-Bowen Orogeny at that time. The Precambrian detrital zircons were likely derived from the Beardmore micro-continent that accreted to the margin of Gondwana in the Cryogenian. Other zircon contributions can be associated with Cambrian aged basement uplifts of the Ross Orogenic Belt and Silurian – Devonian aged basement uplifts of the Lachlan Fold Belt.

The U-Pb age results from this study furthermore highlight a significant shift in provenance during the Late Permian and into the early Triassic sediments with the disappearance of Pre-Carboniferous zircon contributions in the latest Permian. This shift in provenance is thought to reflect changing river dynamics from meandering river systems to braided rivers systems with different sediment calibre transportation

properties. This change is associated with the mass dying of deep-rooted vegetation during the Permian-Triassic mass extinction event.

KEYWORDS

Sydney Basin, Provenance, Permian-Triassic Boundary, Extinction event, U-Pb. Geochronology, Fluvial

TABLE OF CONTENTS

Detrital zircon geochronology of Permian – Triassic fluvial sediments of the Sydney Basin: Provenance analysis and Geomorphological effects of the Permian –Triassic Extinction.....	i
Detrital Geochronology on the P-T boundary of the Sydney Basin	i
Abstract.....	i
Keywords.....	ii
Table of Contents.....	1
List of Figures.....	3
List of Supplementary Figures	3
List of Supplementary Tables.....	4
Introduction	5
Geological Setting	6
Stratigraphy of the Sydney Basin	9
Northern Area	9
Southern Area	11
Tectonic History of Sediment Source Areas	12
Australian Sources	12
New England Fold Belt	12
Lachlan Fold Belt	14
New Zealand Sources.....	14
Tuhua Orogeny.....	14
Antarctic Sources	15
Ross Orogen	15
Beardmore Orogeny.....	16
Sample Discription and Lithology.....	16
Methods	21
Results	22
NS2014002 (early - late Permian Reids Mistake Formation)	22
SY2014004 (early - late Permian Wilton Formation)	22
NS2014008 (late Permian - early Triassic Munmorah Conglomerate).....	22
SY2014010 (late Permian Coalcliff Sandstone)	23
SY2014013 (late Permian - early Triassic Otford Sandstone Member).....	23

SY2014014 (early Triassic Scarborough Sandstone)	23
Discussion.....	24
Provenance Constraints and Sediment Geomorphology in the Late Permian.....	24
Provenance Constraints and Sediment Geomorphology at the P-T Boundary	30
Provenance Constraints and Sediment Geomorphology into the Early Triassic.....	32
Conclusions	33
Acknowledgments	34
References	35
Appendix A:	40
Methods.....	40
Rock Crushing and Mineral Separation	40
Zircon mounting.....	41
LA-ICP-MS and Geochronology	42
Weighted Averages for Provenance Pie Charts	43
NS2014002 – Reids mistake formation	43
SY2014004 – Wilton Formation	44
NS2014008 – Munmorah Conglomerate	44
SY2014010 – Coalcliff Sandstone	45
SY2014013 – Otford Sandstone Member	45
SY2014014 – Scarborough Sandstone.....	46
Raw Data	47
SY2014004	47
Wilton Formation	47
NS2014002.....	48
Reid’s Mistake Formation	48
NS2014008.....	49
Munmorah Conglomerate.....	49
SY2014010	50
Coalcliff Sandstone.....	50
SY2014013	51
Otford Sandstone Member.....	51
SY2014014	52
Scarborough Sandstone	52

LIST OF FIGURES

Figure 1: Generalized geologic structure of southeastern Australia, including sedimentary cover. The Sydney Basin is bound to the North by the New England Orogen and to the west by the Lachlan Orogen.. M.B.=Murray Basin, O.B.= Ottoway Basin, N.E.O.=New England Orogen, D.O.=Delamarian Orogen (modified from Sircombe 1999).....	7
Figure 2: (a) Stratigraphic Log of the northeastern Sydney Basin from the Lake Macquarie/Gosford Area and (b) Stratigraphic Log of the southeastern Sydney Basin from the Wollongong Area. Samples from this study are represented by letters A-F. After (Herbert & Helby 1980; Dehghani 1994; Herbert 1995; Tye <i>et al.</i> 1996; Retallack 1999).....	10
Figure 3: Reconstruction of Gondwana showing the Tasman Orogenic System and its relation to other Orogenic Systems across the Margin of Gondwana after. The Lachlan Fold Belt of Eastern Australia was a consequence of the deformation of this large Orogenic System (modified after Rogers 1993).....	13
Figure 4: Geologic map of the Sydney Basin with indication of sample locations based on 1:250 000 (Sydney) geological map (Brunker & Rose 1969). Samples beginning with 'NS' were collected from the North Sydney Basin; samples beginning with 'SY' were collected from the South Sydney Basin.....	17
Figure 5. (a) Stratigraphic Log of the northeastern Sydney Basin from the Swansea Heads Area. (b) Stratigraphic Log of the southeastern Sydney Basin from the Seacliff Bridge Area. Sample positions have been inserted on their respective sedimentary horizon. After (Ward 1972; Crapp & Nolan 1975; Arditto 1991; Dehghani 1994).....	18
Figure 6. Zircon U-Pb age-frequency diagram, identifying age populations present in the Wilton and Reids Mistake Formations of the Sydney Basin. The U-Pb age spectra displayed here reveal the difference in provenance between the South and North Sydney Basin during the early-Late Permian. The x-axis represents $^{206}\text{Pb}/^{238}\text{U}$ age estimates for ages <1 Ga and $^{207}\text{Pb}/\text{Pb}$ age estimates for ages >1 Ga. (n) is the number of concordant ages within each sample, with a concordance threshold >85%. Each peak records a pulse of magmatism from the sediments' provenance.	25
Figure 7. U-Pb age spectra for the South and North Sydney Basin during the latest Triassic, just before the P-T boundary (see caption for Figure 6),.....	26
Figure 8. U-Pb age spectra for the Late Permian - early Triassic succession of sediments in the South Sydney Basin (see caption in Figure 6).....	27
Figure 9: (A) Pie charts displaying the relative contribution of source terranes based on zircon age peaks (B) U-Pb age spectra of Sydney Basin samples coupled with U-Pb spectra of granites from source regions. Grey shaded areas correlate age peaks from source terranes with the U-Pb spectra of sediments from this study. Data for the Source Terrane Calculations and U-Pb spectra can be found in (Appendix A) All zircon data was filtered by a concordance threshold of >85%. New England Orogen data after Landenberger <i>et al.</i> (1995); Lachlan Fold Belt Data after Keay <i>et al.</i> (1999); New Zealand data after Tulloch <i>et al.</i> (2009b).	30

LIST OF SUPPLEMENTARY FIGURES

Supplementary Figure 1. Weighted Average Plots of U-Pb ages using the $\text{Pb}^{206}/\text{U}^{238}$ age estimates and standard errors (absolute). Bold lines indicate the weighted average of age

estimates that correspond to age peaks of the U-Pb Age Spectra (Figs. 6-8). Weighted averages were used to construct pie charts of relative provenance contribution (Fig. 9). Plots were constructed using Isoplot, after (Ludwig 2012). Weighted average plots of detrital zircons from sample NS2014002 of the early-Late Permian Reids Mistake Formation..... 43

Supplementary Figure 2. Weighted average plots of detrital zircons from sample SY2014004 of the early-Late Permian Wilton Formation (see caption for Supplementary Figure 1) Note: Beardmore and Ross Orogens were incorporated into ‘others’ on the pie chart seen in figure 9a. 44

Supplementary Figure 3. Weighted average plots of detrital zircons from sample NS2014008 of the Late Permian-Early Triassic Munmorah Conglomerate (see caption for Supplementary Figure 1)..... 44

Supplementary Figure 4: Weighted average plots of detrital zircons from sample SY2014010 of the Late Permian Coalcliff Sandstone (see caption for Supplementary Figure 1). 45

Supplementary Figure 5: . Weighted average plots of detrital zircons from sample SY2014010 of the Late Permian Coalcliff Sandstone (see caption for Supplementary Figure 1). 45

Supplementary Figure 6: Weighted average plots of detrital zircons from sample SY2014014 of the Early Triassic Scarborough Sandstone (see caption for Supplementary Figure 1). 46

LIST OF SUPPLEMENTARY TABLES

Supplementary Table 1: Raw U-Pb data from sample SY2014004. (*)Indicates samples that had a concordance threshold value < 85% 47

Supplementary Table 2: Raw U-Pb data from sample NS2014002. (*)Indicates samples that had a concordance threshold value < 85% 48

Supplementary Table 3: Raw U-Pb data from sample NS2014008. (*)Indicates samples that had a concordance threshold value < 85% 49

Supplementary Table 4: Raw U-Pb data from sample SY2014010. (*)Indicates samples that had a concordance threshold value < 85% 50

Supplementary Table 5: Raw U-Pb data from sample SY2014013. (*)Indicates samples that had a concordance threshold value < 85% 51

Supplementary Table 6: Raw U-Pb data from sample SY2014014. (*)Indicates samples that had a concordance threshold value < 85% 52

INTRODUCTION

The Sydney basin, part of the much larger Sydney-Gunnedah-Bowen Basin, is located in New South Wales. The basin formed during the Late Carboniferous to the Early Triassic and preserves a unique record of a full depositional sequence of sediments across the Permian-Triassic Boundary (P-T boundary), which is associated with the most prolific mass extinction event of all time (Veevers *et al.* 1993). Besides the extinction of ~90 % of all marine and terrestrial fauna, the P-T boundary is characterised by significant geomorphological and palaeo-environmental changes as well. Palaeo-environmental changes have been attributed to global warming, wild fires, acid rain, and volcanism associated with the present day Siberian Traps (Benton & Newell 2014; Davies 2015). The combination of these factors fast-tracked the extinction of deep-rooted vegetation, destabilising river banks and leading to greater quantities of sediment run-off from slopes. Evidence of widespread soil erosion has been seen in P-T successions across the globe, where claystone breccias have been found. Retallack (1999) details the presence of these claystone breccias; indicative of wide-spread soil erosion, associated with the mass-dying of deep rooted vegetation. Since deep rooted vegetation has a major control on river morphology (i.e. meandering rivers become braided rivers without the support of roots), it is postulated that significant changes occurred in river morphology at the P-T boundary (Ward *et al.* 2000). Further evidence for mass-dying of deep rooted vegetation and associated major shifts in transport media, depositional style and paleo-environmental conditions at the P-T boundary come from the global disappearance of the coal seams in the earliest Triassic (Retallack *et al.* 1996), particularly on the slopes of river banks and hills Davies (2015). Changes in stratigraphy have been recorded as well in numerous P-T successions around the globe;

Ward *et al.* (2000) noted a shift from fine grain to coarse grain sediments within the Karoo Basin of South Africa and (Davies 2015) has observed a shift from fine grain to coarse grain sediments within the Sydney Basin.

This study reports on detrital zircon geochronological results coupled with sediment facies analyses to constrain the timing of change in fluvial sedimentation across the Sydney Basin at the P – T Boundary. In addition, the results aim to speculate on the provenance of the sedimentary deposits. Sediments of the Sydney Basin have been postulated to come from multiple source terranes including the New England Fold Belt, the Lachlan Orogen, the Ross Orogen and Orogenic Belts of New Zealand (Figure 2; Rust & Jones 1987; Dehghani 1994; Sircombe 1999). This study aims to test whether or not the terranes listed above are plausible source terranes for the Sydney Basin sediments through detrital zircon geochronology using laser-ablation-inductively-coupled mass-spectrometry (LA-ICP-MS). In this regard, the environmental conditions responsible for the weathering and deposition of clastic sediments in the Sydney Basin were analysed before, during and after the P-T Boundary in order to investigate the potential link between the changing palaeo-environmental conditions and the tectonic regime of the hinterland. The provenance results thus provide new constraints on the coupled tectonic-sedimentary history of the Sydney Basin and its relation with the palaeo-environmental change at the P-T boundary in general.

GEOLOGICAL SETTING

The Sydney Basin is outlined in figure 1 and extends approximately 350km along the New South Wales coast and is roughly 180-250km wide. The Sydney Basin, adjacent to the Hunter Valley is proximal to 2 other closely associated basins: the Gunnedah and Bowen Basin. Together they all part of the much larger Sydney-Gunnedah-Bowen

Super-Basin (Gulson et al. 1990). This 2000km long Super-Basin is abutted against the New England Fold Belt to the North and the Lachlan Fold Belt to both the West and South (Figure 1; Jones *et al.* 1984).

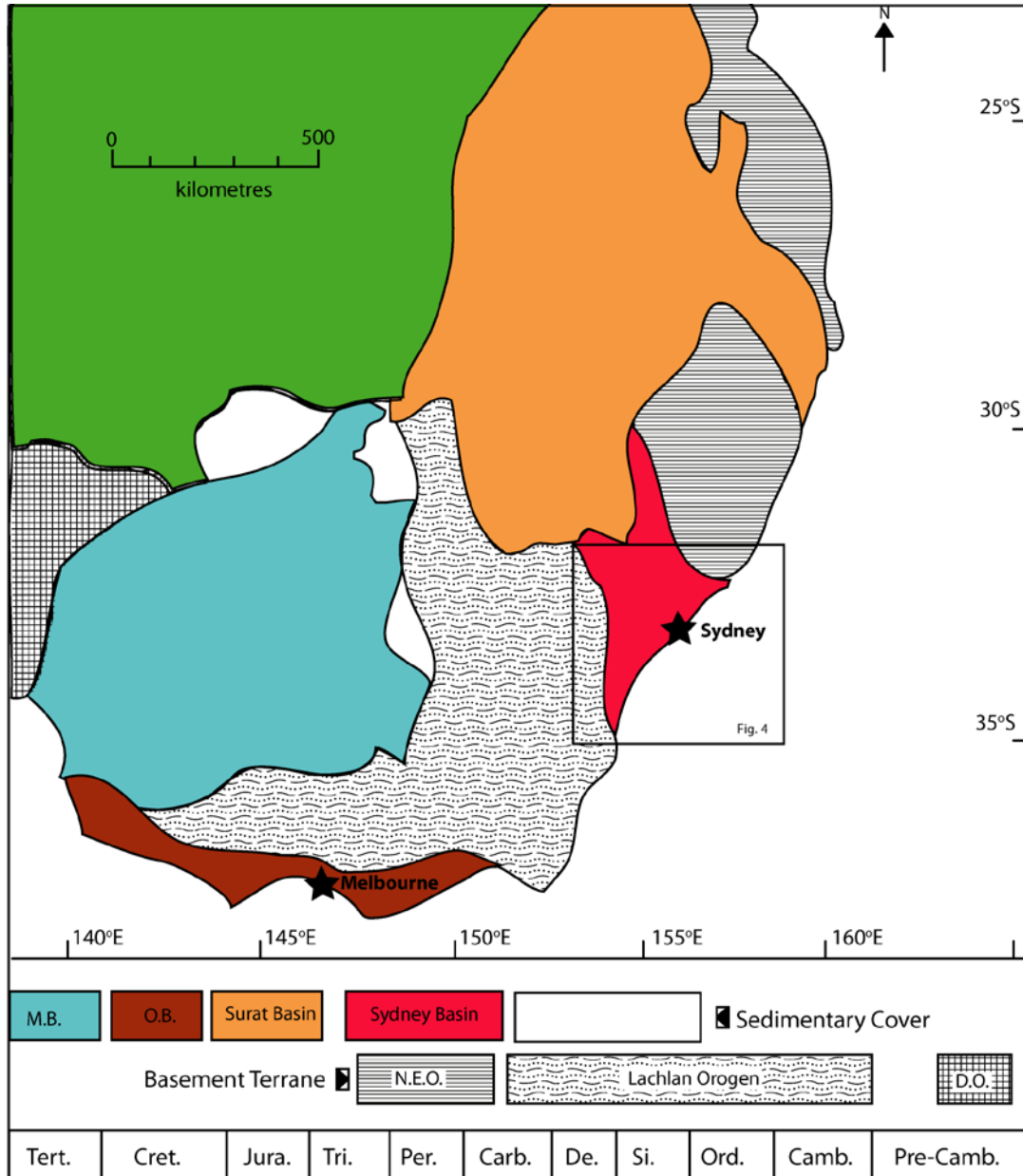


Figure 1: Generalized geologic structure of southeastern Australia, including sedimentary cover. The Sydney Basin is bound to the North by the New England Orogen and to the west by the Lachlan Orogen.. M.B.=Murray Basin, O.B.= Ottoway Basin, N.E.O.=New England Orogen, D.O.=Delamarian Orogen (modified from Sircombe 1999)

The Sydney Basin has been postulated to be a foreland basin (Gulson et al. 1990) that likely formed after rifting and back arc-volcanism of the Hunter-Bowen Orogeny in the early Permian. However, Wightman *et al.* (1994) that the Sydney Basin is a strike-slip basin located at a convergent margin. Clastic deposition into the Basin is thought to be largely molassic and began in the late-Early Permian and ceased in the middle Triassic (Figures 2a, b).

The estimated thickness of the Sydney Basin sediments is ~5000m at the northern Margin, however, this thickness is reduced to two-thirds towards the southernmost regions of the basin (Herbert & Helby 1980). Substantial erosion has occurred between sedimentary packages, especially close to the P-T Boundary with only a few remaining areas preserving the full sequence of clastic deposition (Dehghani 1994). Sedimentation was initially slow in the early Permian, and fluctuated rapidly throughout the middle to late Permian (Herbert 1995). Sedimentation rates increased substantially towards the P-T Boundary to an elevated rate of 65m/Ma (Gulson et al. 1990). The shift to terrestrial sedimentation dominated by fluvial environments, as discussed below, likely accounts for an increase in sedimentary yield at the P-T Boundary.

The Basin itself hosts some of the largest coal deposits seen in eastern Australia. Coal seams from a few metres to 100's of meters are present within the sedimentary record of the basin, indicative of once lush vegetation dominating the Permian landscapes (Hunt 1988; Davies 2015) has indicated that the absence of coal seams in the early Triassic are probably a result of vegetation decrease associated with the P-T extinction event. The first emergence of coal seams within the Triassic came ~15-20 million years after the P-T Boundary (Davies 2015). Prior to the first Triassic coal exposures, sediments were generally coarse grained and lacked fossil content (Figure 2). This is in

substantial contrast with the strata deposited prior to the P-T Boundary, where sediments accumulated in marine to coastal marine environments, associated with a eustatic sea level rise and basin subsidence (Dehghani 1994). The sudden shift from Permian molasse deposits to Triassic fluvial and alluvial sediments suggests a rapid change in palaeo-environmental conditions at the P-T boundary.

The following sections summarise the stratigraphy of the basin and the tectonic evolution of the hinterland to provide constraints for provenance analysis for the Sydney Basin sediments.

STRATIGRAPHY OF THE SYDNEY BASIN

Northern Area

The *Dalwood Group* is composed of four sedimentary formations (Figure 2b), the mafic volcanics of the *Lochinvar Formation* (Gulson *et al.* 1990), the *Rutherford Formation* and the *Farley Formation* (Gostin & Herbert 1973). The presence of marine fauna within the *Dalwood Group* indicates marine influences on sedimentation in the early Permian. The *Dalwood Group* was succeeded by the *Greta Coal Measures* that are composed of coal seams, sandstones, siltstones, conglomerates and indicate a mixed fluvial-marine depositional history (Dragovich & Patterson 1995; Herbert 1995).

Overlying the *Greta Coal Measures* is the late-Early Permian *Maitland Group*, composed of marine formations (*Branxton* and *Mulbring Formations*) that bracket the *Muree Sandstone*, a fluvial-near shore deposit (Glen & Beckett 1997). Following the *Maitland Group* are the middle-late Permian *Newcastle Coal Measures*. The *Newcastle Coal Measures* contain sandstones, shales, cherts, conglomerates and coal seams and

were deposited in a series of alternating coastal plain and marine-shelf palaeo-environments (Herbert 1995).

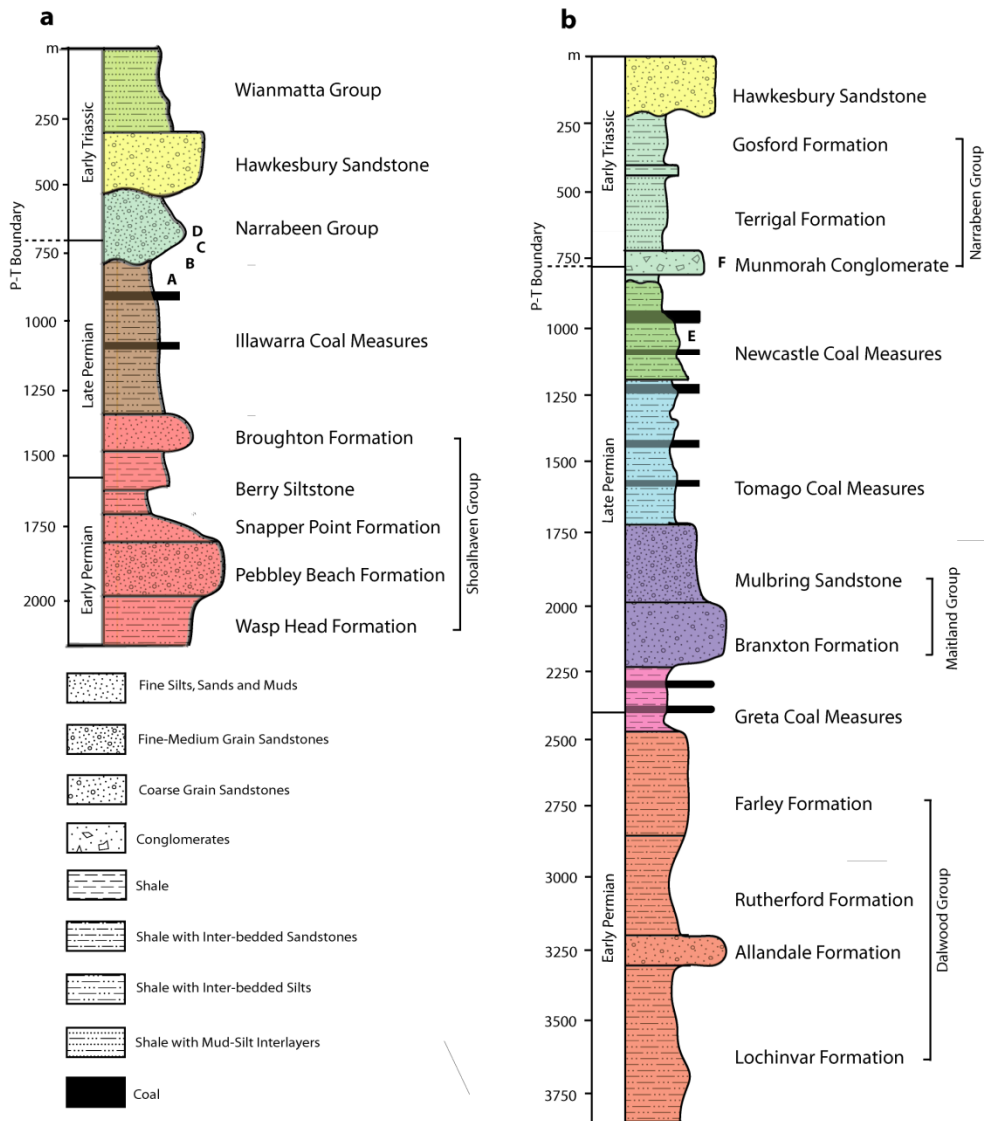


Figure 2: (a) Stratigraphic Log of the northeastern Sydney Basin from the Lake Macquarie/Gosford Area and (b) Stratigraphic Log of the southeastern Sydney Basin from the Wollongong Area. Samples from this study are represented by letters A-F. After (Herbert & Helby 1980; Dehghani 1994; Herbert 1995; Tye *et al.* 1996; Retallack 1999)

The base of the *Narrabeen Group* represents an erosional unconformity above the *New Castle Coal Measures* (Figure 2b). The basal layers of the *Narrabeen Group* are represented by the *Dooralong Shale* and *Munmorah Conglomerate*. The *Dooralong Shale* is composed of fine silts and sands deposited in an fluvial-estuary environment

while the *Munmorah Conglomerate* contains abundant angular fragments and pebbles showing similarities to alluvial fan deposits (Diessel 1992). Following the *Narrabeen Group* is the Early Triassic *Hawkesbury Sandstone*, a quartz-lithic arenite containing abundant pebbly fragments. Overlying the *Hawkesbury Sandstone* is The *Wianamatta Group*; composed of greywacke-sandstones and shales deposited in shallow-deep marine palaeo-environment; marking the cessation of sedimentation in the Sydney Basin (Lovering 1953).

Southern Area

Deposition of sediments within the Southern Sydney Basin begun with the *Shoalhaven Group* in the early Permian (Figure 2a). The *Shoalhaven Group* encompasses the Wasp Head Formation, Pebbly Beach Formation, Snapper Point Formation, *Berry Siltstone* and the *Broughton Formation*. Tye *et al.* (1996) suggests the entire depositional sequence of the *Shoalhaven Group* records an extensional phase of the Basin in which marine sediments dominated the early Permian stratigraphy.

Overlying the *Shoalhaven Group* are the fine silts, sands and coal seams of the *Illawarra Coal Measures*. Unconformably overlying the Illawarra Coal measures are the basal layers of the Narrabeen Group; the Coalcliff Sandstone; the Wombarra Claystone and the Scarborough Sandstone. The Coalcliff Sandstone of the late-Permian is composed of quartz-lithic sandstones and thin grey claystones; the *Wombarra Claystone* is composed of massive claystones and siltstones and the *Scarborough Sandstone* is composed of quartz-lithic sands with abundant pebbly fragments (Jakeman 1980; Dehghani 1994). The *Scarborough Sandstone* contains the most coarse-grain sediments seen within the Early Triassic succession of the *Narrabeen Group*.

TECTONIC HISTORY OF SEDIMENT SOURCE AREAS

Australian Sources

NEW ENGLAND FOLD BELT

The New England Fold Belt (NEFB) is a late Phanerozoic - early Palaeozoic mountain belt located directly to the North of the Sydney Basin, on the coastline of New South Wales (Figure 1). This particular fold belt is divided into two segments; the northern and southern New England Fold Belts separated by younger sedimentary cover sequences (Collins 1991; Sircombe 1999). The NEFB is defined by a series of accretionary complexes including a westward volcanic chain, a fore-arc basin and an eastern non-volcanic arc-platform trench complex (Veevers *et al.* 1993). From the Silurian-Devonian active magmatism convergent deformation margin generated a westward-oriented intra-oceanic island arc (Aitchison *et al.* 1992). Early-Middle Devonian times emplaced this intra-oceanic arc (Gamolaroi Terrane) onto the margin of Eastern Australia, along with subduction-accretion complexes and the Tamworth Belt (Offler & Gamble 2002). Early Carboniferous history of the NEFB involved the deposition of volcanoclastic sediments from the Tamworth Belt in a fore-arc setting prior to uplift and metamorphism. The tectonic regime during the Carboniferous was primarily a west-ward dipping subduction zone, inducing convergent deformation throughout the belt up until the early Permian (Murray *et al.* 1987). From this point convergent tectonics halted and either (a) slab roll back (Leitch 1975; Watanabe *et al.* 1988) or (b) quantum tectonics (Aitchison & Buckman 2012) caused a phase of extension in the onset of the Permian, initiating the first sediments to collect and form the basal layers of the Sydney Basin (Veevers & Morgan 2000). Extensional deformation was short lived as the Hunter-Bowen Orogeny deformed the southern

NEFB during the middle Permian - Mid Triassic (Collins 1991; Holcombe *et al.* 1997). Sediments within the Sydney Basin are mostly likely related with the eroded detrital material of granitic suites emplaced during pulses of magmatism in the New England Fold Belt. (Holcombe *et al.* 1997). Granitic clasts dated in conglomerates within the central regions of the orogen have presented ages of 344-340 Ma (Green 1973). Permian S-Type granites were emplaced between 289-286 Ma (Flood & Shaw 1977) and I-Type granites, emplaced between 262-225 Ma (Shaw & Flood 1981; Mensel *et al.* 1985). In the southern NEFB, these are represented by the calc-alkaline Bundarra and Hillgrove suites as well as the New England Batholith, with ages ranging between 350-225 Ma (Green & Kridoharto 1975; Sircombe 1999).

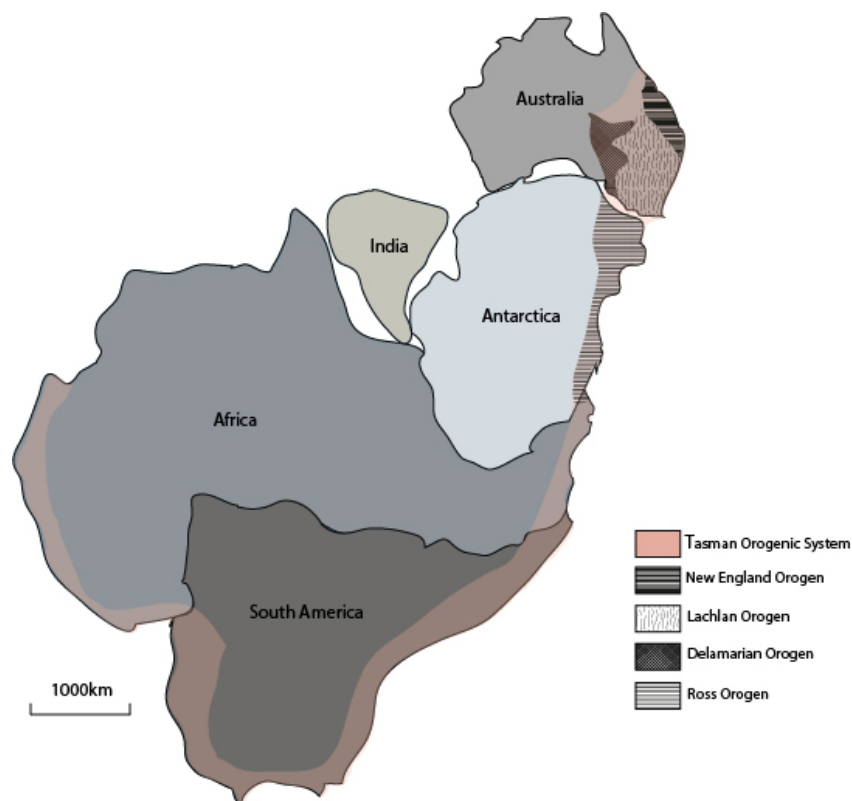


Figure 3: Reconstruction of Gondwana showing the Tasman Orogenic System and its relation to other Orogenic Systems across the Margin of Gondwana after. The Lachlan Fold Belt of Eastern Australia was a consequence of the deformation of this large Orogenic System (modified after Rogers 1993).

LACHLAN FOLD BELT

The Lachlan Fold Belt (LFB) is a 700km wide orogenic belt, part of the much larger Tasman Orogenic System, defined by continuous micro-continent collisions of arc systems along margin of eastern Australian Margin (Figure 3). The LFB is thought to be an ‘accretionary orogeny’ as there is little observed evidence of a continent-continent collision (Scheibner 1973; Veevers & Morgan 2000). The belt is composed of shallow marine sedimentary rocks, turbidites, cherts and calc-alkaline volcanic rocks (Gray 1997; Foster & Gray 2000). Pulses of tectonic activity occurred between 450-340 Ma, resulting in a volcanic and plutonic complex intruding existing Cambrian - Ordovician sediments and deforming them (Gray & Foster 1997; Sircombe 1999). The plutonic complex is composed of a number of distinct granite batholiths all aged between 440-360 Ma (Williams 1992). Gray (1997) and Sircombe (1999) have shown the existing detrital relationship between Permian - Triassic sediments in the Sydney Basin and granitic and volcanic suites of the Lachlan Orogen. These sediments include the early Permian *Tallong Conglomerate* from the *Shoalhaven Group* (Figure 2a); the early-Triassic *Terrigal Formation* from the *Narrabeen Group* (Figure 2b) and the Mid-Triassic *Hawkesbury Sandstone* (Figure 2a). Detrital geochronology within this study aims to provide more detailed constraints on the links between magmatism and deformation in the LFB and sedimentation in the Sydney Basin.

New Zealand Sources

TUHUA OROGENY

The Tuhua Orogeny uplifted, deformed and metamorphosed the Western Province of New Zealand during the middle-Palaeozoic. Deformation effected Ordovician

greywackes from the Buller Terrane; Cambrian Volcanics; Ordovician siliclastic rocks from the Takaka Terrane and high-grade rocks from the Fjordland (Gibson 1992). Gibson (1992) and Tulloch *et al.* (2009a) demonstrated the similarities between Palaeozoic magmatism from the Western Province of New Zealand and magmatism from both the Lachlan Fold Belt and the trans-Antarctic Mountain Ranges. Granitic suites seen within Western Province include the Karamea Suite (~355-340 Ma); Paringa Suite (~369-362 Ma); Ridge Suite (~354-340) and the Tobin Suite (~350-342 Ma). These granitic suites intruded argillites and greywacke turbidites of the Greenland Group throughout the early Devonian (Scott *et al.* 2011).

Antarctic Sources

ROSS OROGEN

The Ross Orogeny was part of the coupled Ross-Delamarian Orogeny that deformed Antarctica and south Australia during the Cambrian (Sircombe 1999). This orogeny is essentially a consequence of convergent tectonics from the Neoproterozoic to the early Phanerozoic assembling the super-continent Gondwana via the Tasman Orogenic System, leading to the generation of the Trans-Antarctic Mountain ranges (Federico *et al.* 2009).

A previous detrital study on the Hawkesbury Sandstone in the Sydney basin eluded to the presence of Neoproterozoic - Early Cambrian detrital zircon grains (Sircombe 1999). These detrital zircons exceed any relations with magmatism in the Lachlan Fold Belt, however, previous detrital and paleo-directional studies have indicated Ordovician turbidites of the Lachlan Orogen have been sourced from the south – south west, correlating with the uplift of the Ross-Delamarian Orogeny (Cas *et al.* 1980; Cas 1983;

Williams *et al.* 1994). It has been suggested that recycling of Neoproterozoic-Early Cambrian zircon grains occurred throughout the Lachlan Orogeny, as there is no evidence of a sedimentary pathway between the Trans-Antarctic Mountain Ranges and the Sydney Basin during the Permian-Triassic (Cowan 1993; Sircombe 1999).

BEARDMORE OROGENY

In the late Neoproterozoic, oblique subduction of the Paleo-Pacific beneath Antarctica caused shear deformation to the Trans-Antarctic Mountain Range, resulting in the amalgamation of the allochthonous Beardmore Microcontinent to the east Antarctic Craton (Veevers 2003). A reported detrital zircon age from mafic igneous rocks of the Beardmore Group gives an age estimate of 668 \pm 1 Ma (Goodge *et al.* 2002), suggesting the Beardmore Orogeny may have also been responsible for the widespread appearance of Neo-Proterozoic grains in Palaeozoic sediments (Sircombe 1999). The exact timing of this orogenic event is unclear; ages in the late Neoproterozoic (~650 Ma) have been reported (Grindley & McDougall 1969; Laird 1991) but have subsequently been challenged (Stump *et al.* 1986; Pankhurst *et al.* 1988; Stump *et al.* 1991). Nonetheless, the presence of a Cryogenian - Ediacaran Orogenic event in the Trans-Antarctic Mountain Range is clear.

SAMPLE DESCRIPTION AND LITHOLOGY

Samples were collected from beach outcrops and road cuttings from 2 study areas, each recording the transition from Permian-Triassic sedimentation of the retro-arc-foreland Sydney Basin (Figure 4).

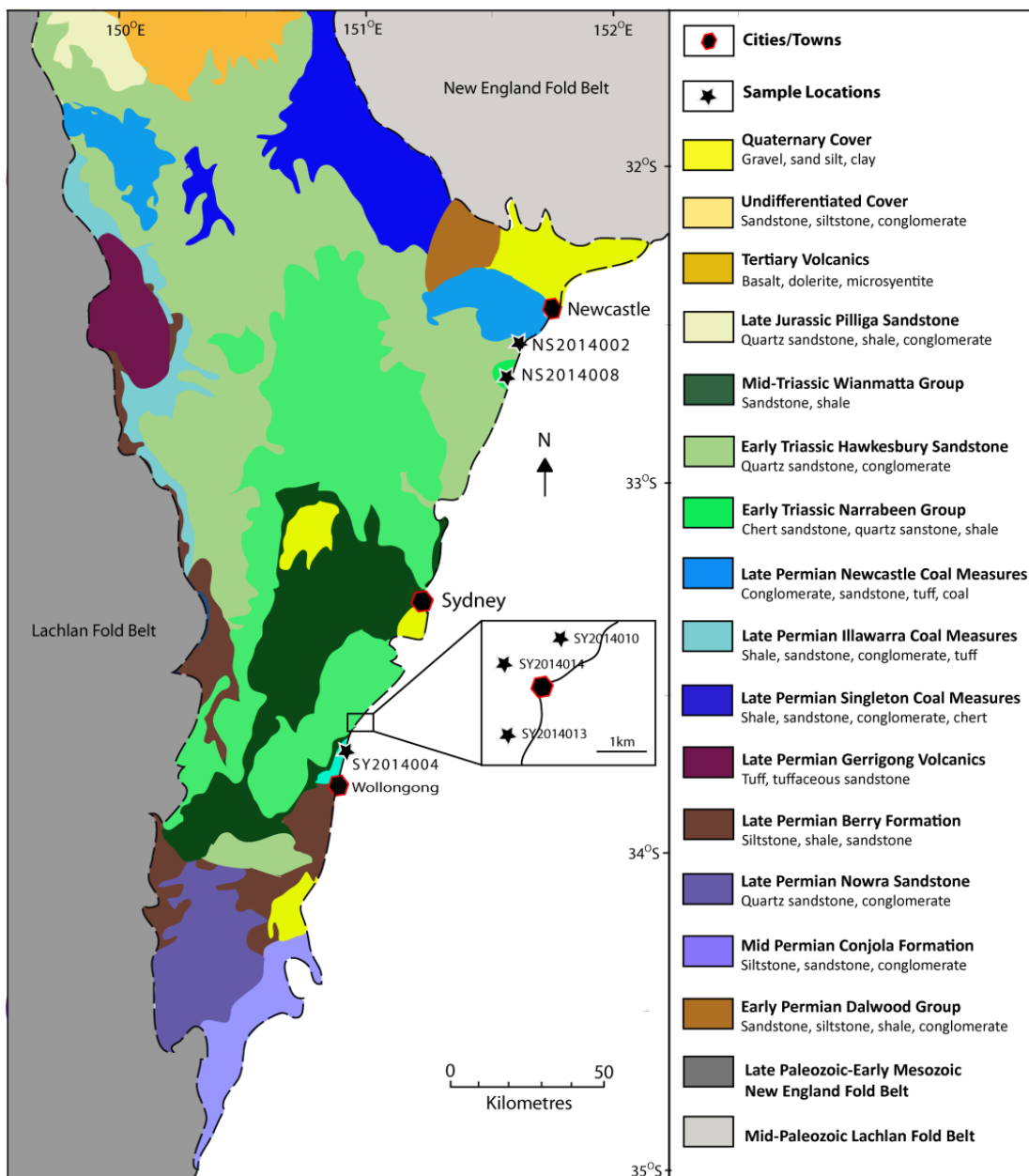


Figure 4: Geologic map of the Sydney Basin with indication of sample locations based on 1:250 000 (Sydney) geological map (Brunker & Rose 1969). Samples beginning with 'NS' were collected from the North Sydney Basin; samples beginning with 'SY' were collected from the South Sydney Basin.

Samples NS2014008 and NS2014002 were both taken from the northern region of the Basin, close to Newcastle. Both samples are Permian in age with NS2014008 representing the last Permian unit of the Northern Sydney Basin (Davies 2015).

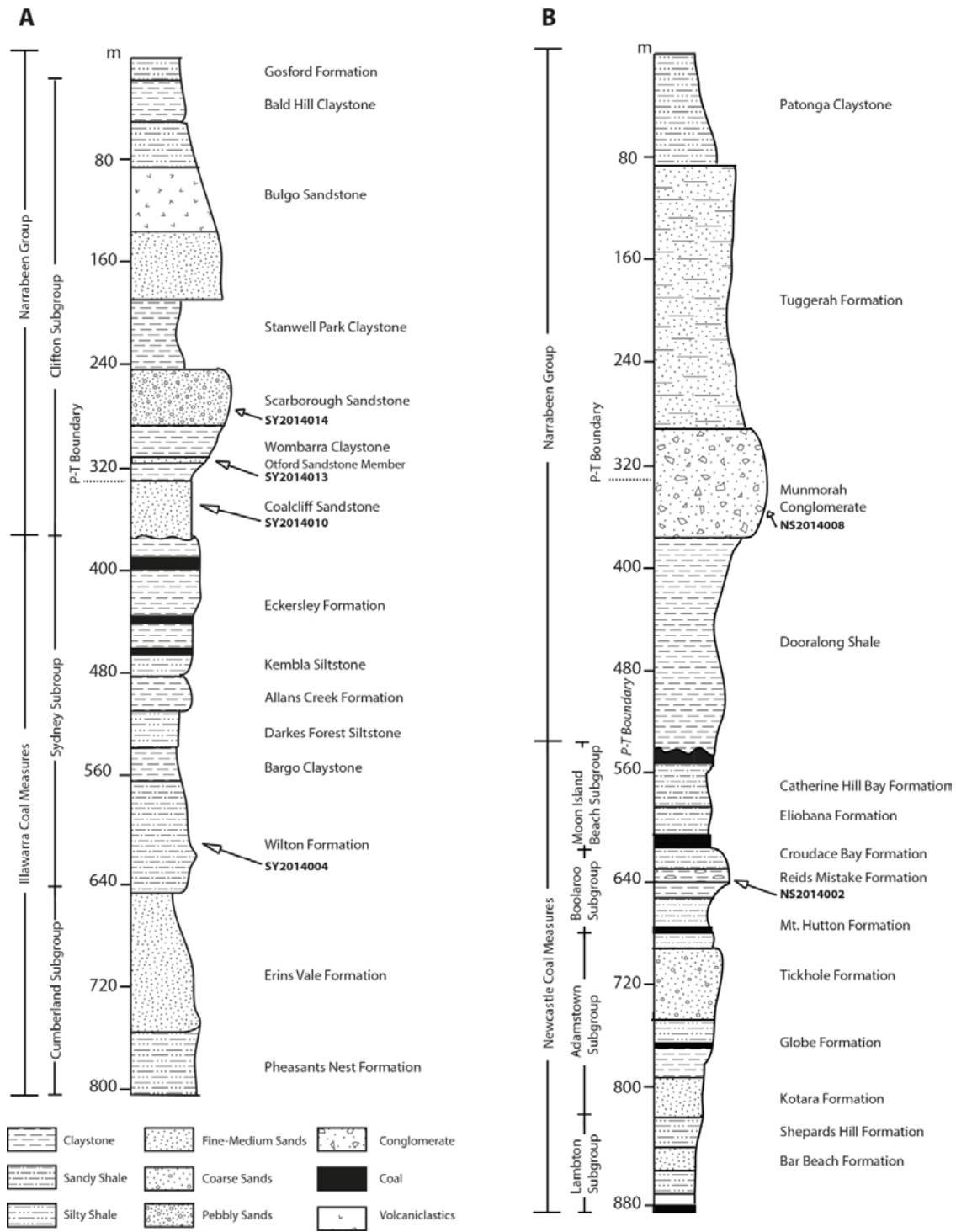


Figure 5. (a) Stratigraphic Log of the northeastern Sydney Basin from the Swansea Heads Area. (b) Stratigraphic Log of the southeastern Sydney Basin from the Seacliff Bridge Area. Sample positions have been inserted on their respective sedimentary horizon. After (Ward 1972; Crapp & Nolan 1975; Arditto 1991; Dehghani 1994)

Sample NS2014002 was taken from the 7 metre thick tuffaceous unit of the *Reids*

Mistake Formation (Figure 5), from beachfront outcrops at Swansea Heads. The *Reids*

Mistake Formation forms part of the 120 metre thick *Boolaroo Subgroup* (Shi & McLoughlin 1997). This formation is a 7 metre thick succession of weathered volcanic tuffs, cherty sandstone, carbonaceous shale and distinctive upper-lower coal seams (Wadia 2015). Herbert (1995) has identified the *Reids Mistake Formation* as being deposited following a period of maximal transgression, limiting the input of clastic sediment and preserving input of air-fall and base-surge tuffs.

The *Munmorah Conglomerate*, part of the *Narrabeen Group*, containing the succession of sediments across the P-T Boundary in the Northern Sydney Basin. Sample NS2014008 was collected from a road-side outcrop of the *Munmorah Conglomerate* along Snapper Point Road, ~20km south of Swansea Heads (Figure 4). It consists of ‘grey lithic-quartz sandstone’ containing pebbly fragments up to 50mm in diameter (Retallack 1999). The sharp angular lithic fragments seen within this sample, coupled with the erosional nature of the *Munmorah Conglomerate* at the P-T Boundary, indicate deposition in a high energy – high slope palaeo-environment of an alluvial fan (Dehghani 1994).

In the South Sydney Basin, SY2014004 was sampled from a horizon within the *Wilton Formation* (Figure 5), located near the sea-side suburb of Thirroul, NSW. The *Wilton Formation* is part of the much larger depositional system of the *Illawarra Coal Measures* and is composed of dark claystones and siltstones, interbedded with sandstone towards the upper half of the formation (Hutton & Bamberry 1999; Hutton 2009).

The presence of upwards-coarsening sequences along with laterally extensive carbonaceous layers suggest a depositional environment of deltaic plains in the lower

reaches of river-dominated deltas. This depositional environment is analogous to the modern Mississippi River Delta (Hutton & Bamberry 1999).

Samples SY2014010 and SY2014013 were taken from the late Permian Coalcliff Sandstone and Otford Sandstone Member (Wombarra Claystone) of the Narrabeen Group (Figure 5), collected towards the southern margins of the Basin at Seacliff Bridge (Figure 4). The Coalcliff Sandstone is a well to moderately well sorted quartz lithic sandstone interpreted to be a fluvial channel deposit. The Wombarra Claystone contains mid-green, green-grey claystones with inter-bedded sandstone units, comprising the Otford Sandstone Member. The Wombarra Claystone records deposition in a lacustrine environment (Moffitt 2000).

A basin wide erosional surface after the Wombarra Sandstone has been observed, culminating in the Scarborough Sandstone (Cowan 1993; Dehghani 1994). Sample SY2014014 was collected at Seacliff Bridge from the Scarborough Sandstone and contains abundant pebbly fragments with limited fine grain sediment input. This erosional sequence, has been correlated with the early Triassic Digby alluvial system of the Bowen Basin, suggesting a more regional evolution of depositional environment (Hamilton 1991; Hamilton & Tadros 1994). The contact between the Wombarra Sandstone and the Scarborough Sandstone is now referred to as the Permian-Triassic Boundary due to a distinct lithofacies change (Arditto 1991). The broad dispersal of this sedimentary package was due to the truncation of sediments in the basin, eroding underlying strata from the North and redepositing them in the South. There is strong suggestion that the progradation of the river delta responsible for the deposition of the Munmorah Conglomerate in the North Sydney Basin re-eroded conglomeratic material; with detritus migrating South-wards across the surface area of the basin (Dehghani

1994). The Scarborough Sandstone records a large braided river complex, shallow in depth but laterally extensive (up to seven hundred metres wide).

METHODS

The applied methodology for zircon U-Pb dating is outlined in (Wade *et al.* 2008; Payne *et al.* 2013). Zircons were concentrated using conventional methods involving magnetic and heavy liquid separation techniques (Appendix A). From those separates, ~120 zircon grains were randomly selected, picked and placed onto glass slides and mounted in epoxy resin. Each mount was carbon coated by Adelaide Microscopy Staff for cathodoluminescence imaging (on the FEI Quanta600 Scanning Electron Microscope) to reveal the internal structure of the zircon grains.

Subsequently, the zircons were analysed for their Uranium and Lead isotopic composition using an Agilent 7500cx attached to a New Wave UP-213 laser ablation system at Adelaide Microscopy. The laser was calibrated to fire 30um spots in the centre of selected zircon surfaces. A nominal fluency value of 5.0J/cm² and laser frequency of 5Hz were used. The standard GJ-1 was used to correct for instrument drift, and was measured multiple times throughout each ablation session (Jackson *et al.* 2004). Plešovice zircon was used as an accuracy check (Sláma *et al.* 2008). Zircon analysis with >15% discordancy were rejected to refine the data. Data reduction was performed using GLITTER (Neufeld) and U-Pb ages were calculated using Isoplot (Ludwig 2012). Zircon U-Pb age frequency diagrams with Kernel Density Estimates were produced via Peter Vermeesh's software 'Density Plotter' (Vermeesch 2012). An extended methods section is provided in Appendix A.

RESULTS

NS2014002 (early - late Permian Reids Mistake Formation)

Out of 80 analysed detrital zircons, only 59 presented concordant ages with a discordancy threshold of $\leq 15\%$. Two age populations are present; ~ 300 - 360 Ma representing $\sim 75\%$ of all analysed zircons and another minor peak at ~ 280 - 240 Ma representing $\sim 20\%$. In addition, two outliers of ~ 600 - 700 Ma were obtained (Figure 6). The most probable ^{206}Pb - ^{238}U age of the Nth-youngest concordant detrital grain is 240.83 ± 15 Ma; this value is interpreted as the maximum deposition age.

SY2014004 (early - late Permian Wilton Formation)

Out of 81 detrital zircon grains analysed, 61 were concordant following a discordancy threshold of $\leq 15\%$. Four main age populations can be distinguished at ~ 700 - 620 Ma (10%); ~ 520 - 460 Ma (20%); ~ 450 - 400 Ma (40%); ~ 310 - 290 Ma (20%, Figure 6). A minor peak is shown at ~ 1200 - 900 Ma, but contains too few zircons to be a reliable source terrane. The most probable ^{206}Pb - ^{238}U age of the Nth-youngest concordant detrital grain is 256.25 ± 9.9 Ma; this value is interpreted as the maximum deposition age.

NS2014008 (late Permian - early Triassic Munmorah Conglomerate)

Out of 80 detrital zircon grains analysed, 47 were concordant following a discordancy threshold of $\leq 15\%$. Two main age populations are present; $\sim 70\%$ of all analysed zircons are attributed to an age peak of ~ 380 - 320 Ma and $\sim 25\%$ attribute to an age peak of ~ 280 - 240 Ma (Figure 7). A single older zircon grain gives an age estimate of 900 Ma.

The most probable ^{206}Pb - ^{238}U age of the Nth-youngest concordant detrital grain is 238.33 ± 35 Ma; this value is interpreted as the maximum deposition age.

SY2014010 (late Permian Coalcliff Sandstone)

Out of 80 detrital zircon grains analysed, 76 were concordant following a discordancy threshold of $\leq 15\%$. The U-Pb age spectra displays two dominant age peaks of ~ 360 - 300 Ma (80%) and ~ 260 - 240 Ma (10%) and few older (early Palaeozoic – Neoproterozoic) zircon ages (maximum age of ~ 650 Ma, Figure 7). The most probable ^{206}Pb - ^{238}U age of the Nth-youngest concordant detrital grain is 240.42 ± 10 Ma; this value is interpreted as the maximum deposition age.

SY2014013 (late Permian - early Triassic Otford Sandstone Member)

Out of 80 detrital zircon grains analysed, 47 were concordant following a discordancy threshold of $\leq 15\%$. A number of age populations are present within this sample; ~ 370 - 310 Ma and ~ 280 - 240 Ma (Figure 8). Two older zircon grains record their own respective peaks at ~ 550 and ~ 450 Ma record their own individual minor peaks respectively. This sample again records a Permian detrital population as well as a Carboniferous population, correlating the similar peaks seen in NS2014002, NS2014008, SY2014004 and SY2014010. The most probable ^{206}Pb - ^{238}U age of the Nth-youngest concordant detrital grain is 245.33 ± 8.2 Ma; this value is interpreted as the maximum deposition age.

SY2014014 (early Triassic Scarborough Sandstone)

Out of 80 detrital zircon grains analysed, 76 were concordant with a discordancy threshold of $\leq 15\%$. A number of age populations are present within this sample; ~ 370 -

310 and 280-240 (Figure 8). SY2014014 is unique in that the histogram of ages 240-260 exceeds that of the Kernel Density Curve, thus the proportion of ages seen in the younger age grouping was far greater than that of any other another sample in this study. SY2014014 records distinct Permian and Carboniferous age peaks that have been seen in all samples within this study. The most probable ^{206}Pb - ^{238}U age of the Nth-youngest concordant detrital grain is 236.87 ± 11 Ma; this value is interpreted as the maximum deposition age.

DISCUSSION

Provenance Constraints and Sediment Geomorphology in the Late Permian

The position of the age peaks for the two early-Late Permian *sediments Reids Mistake Formation* (NS2014002) and the *Wilton Formation* (SY2014004) share similar peaks Permian age (~260 Ma) however, in sample SY2014004, this Permian peak is ~20 Ma older than the Permian peak in NS2014002. Furthermore, the relative abundance of Permian zircons is also significantly higher in SY2014004 than NS2014002 (Figure 9). Deposition of SY2014004 occurred before NS2014002, suggesting that late Permian (~255 Ma) granitic material had not yet been uplifted during deposition of SY2014004. Instead, an abundance of older, mid-Permian detritus was available for erosion. There is a noticeable lack of Carboniferous zircons (~330 Ma) seen in sample SY2014004 compared to NS2014002. Figure 9b shows the correlation between Carboniferous zircons and granitic material of New Zealand, suggesting granites of the New Zealand Tuhua Orogeny were not exposed and thus available for erosion during deposition of the *Wilton Formation*.

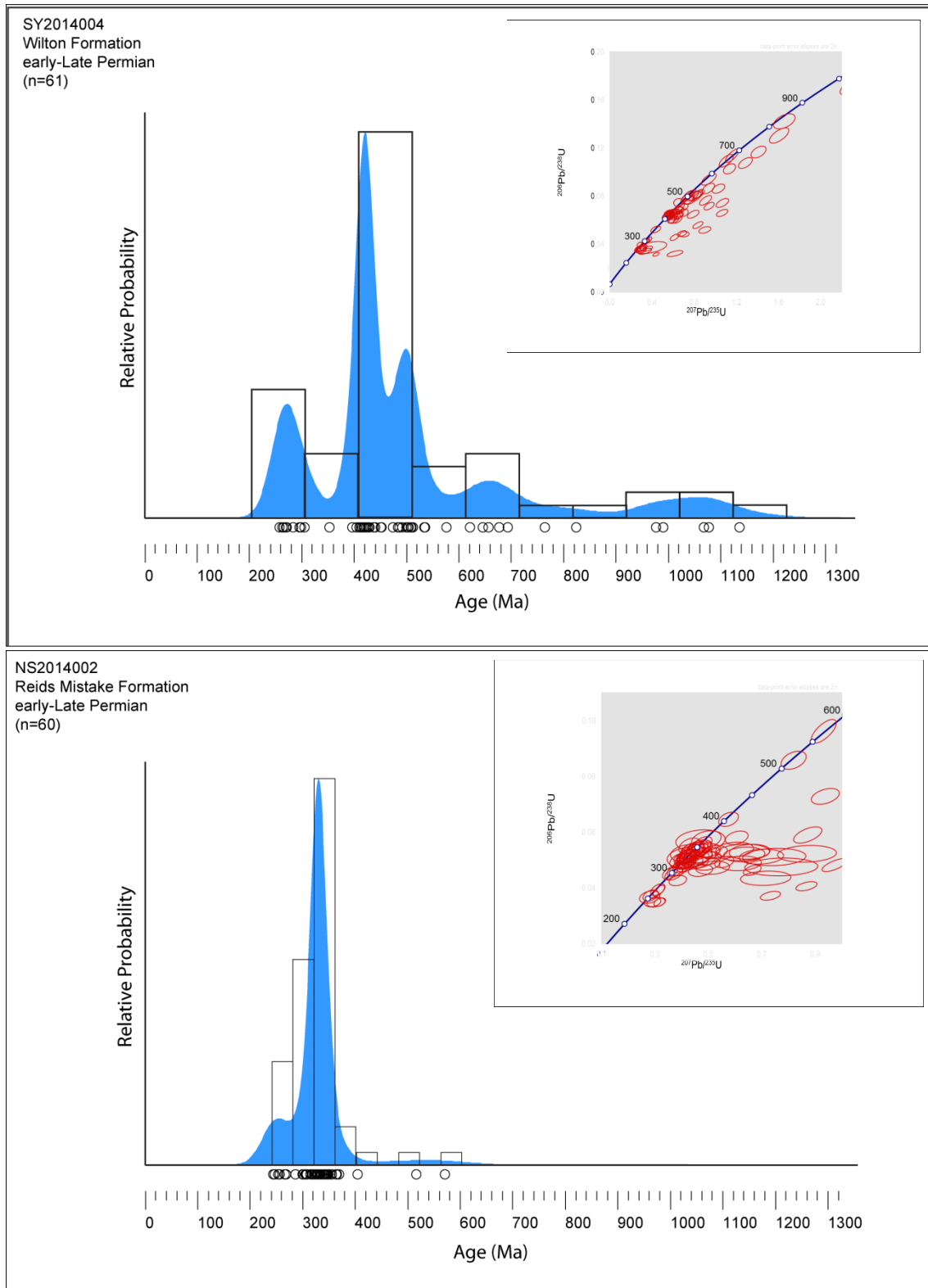


Figure 6. Zircon U-Pb age-frequency diagram, identifying age populations present in the Wilton and Reids Mistake Formations of the Sydney Basin. The U-Pb age spectra displayed here reveal the difference in provenance between the South and North Sydney Basin during the early-Late Permian. The x-axis represents $^{206}\text{Pb}/^{238}\text{U}$ age estimates for ages <1 Ga and $^{207}\text{Pb}/^{235}\text{U}$ age estimates for ages >1 Ga. (n) is the number of concordant ages within each sample, with a concordance threshold >85%. Each peak records a pulse of magmatism from the sediments' provenance.

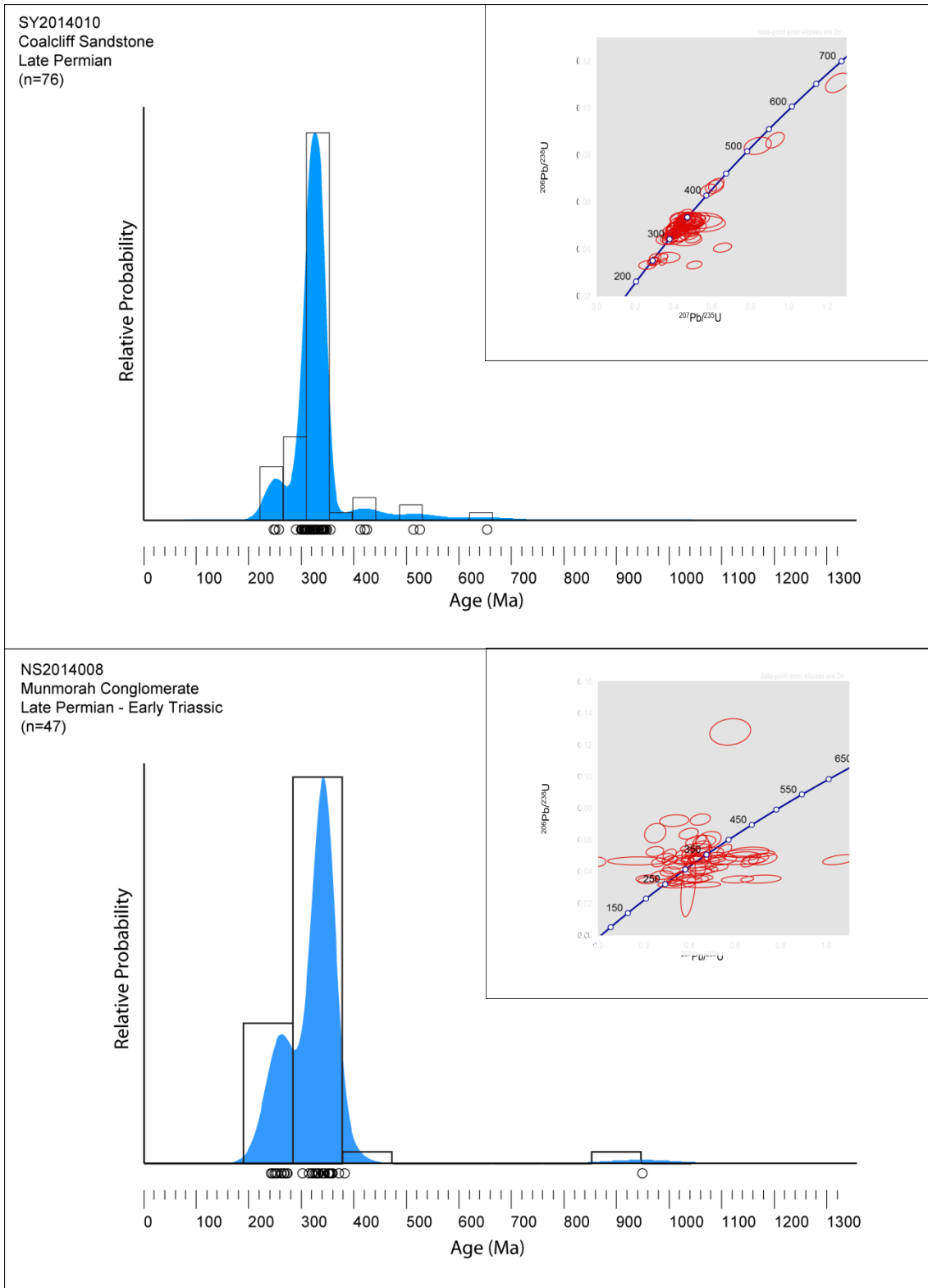


Figure 7. U-Pb age spectra for the South and North Sydney Basin during the latest Triassic, just before the P-T boundary (see caption for Figure 6),

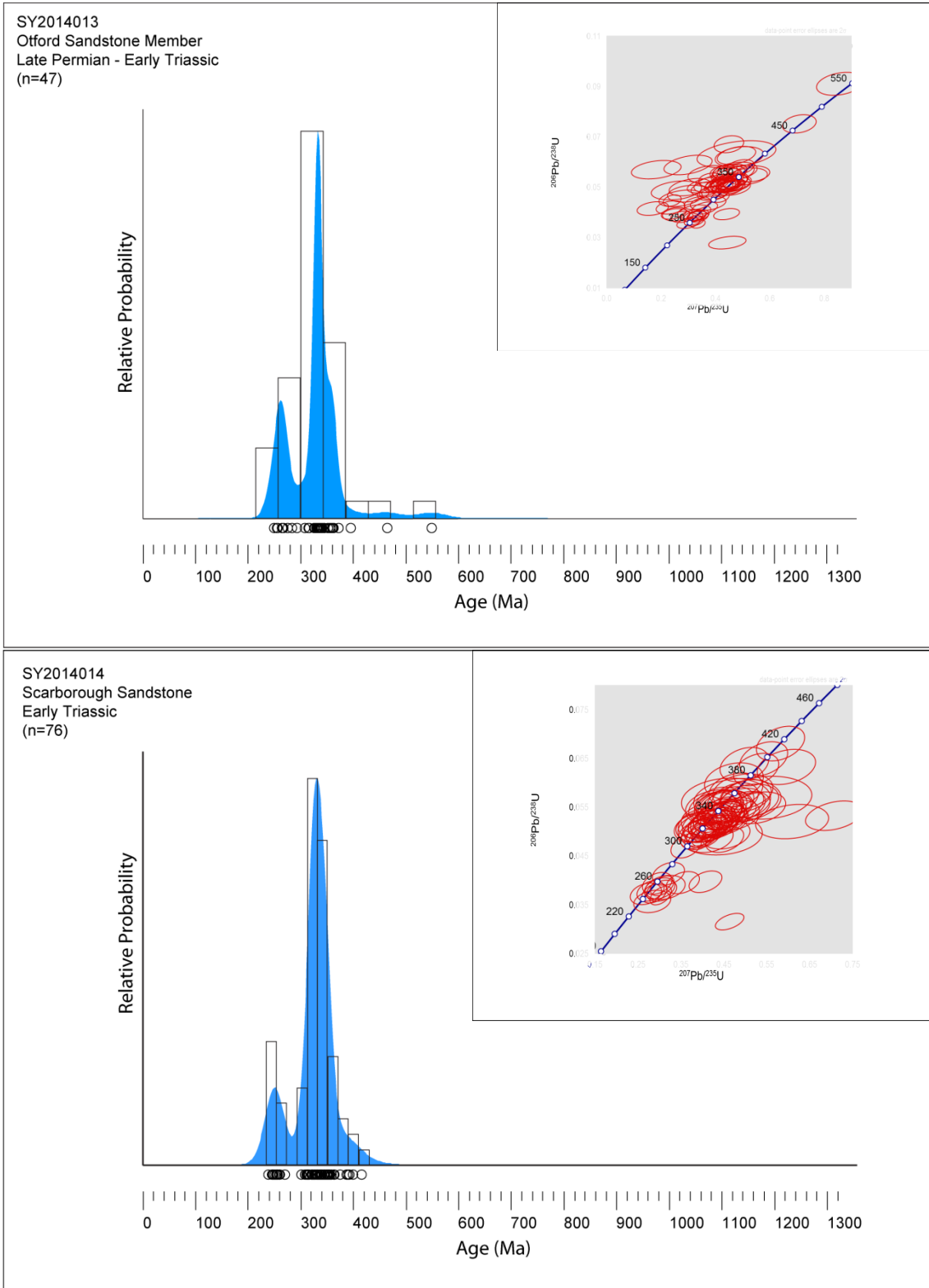


Figure 8. U-Pb age spectra for the Late Permian - early Triassic succession of sediments in the South Sydney Basin (see caption in Figure 6)

The abundance of Carboniferous zircons seen in all sediments in this study after deposition of the *Wilton Formation* indicates a significant provenance change from the New England Orogen to the Tuhua Orogen in the Late Permian sediments of the Sydney Basin (Figure 9a). Further evidence of a provenance shift is indicated by the presence of a Cryogenian peak (~650 Ma); a Cambrian peak (~504 Ma) and a Silurian-Devonian peak (~417 Ma) within the U-Pb spectra of SY2014004. Age peaks of Cryogenian (~650 Ma) and Cambrian (~504 Ma) age are associated with the exhumation and erosion of the Beardmore Orogens and Ross respectively, however, there is no evidence of a sedimentary pathway between Antarctica and the Sydney Basin during the early-Late Permian (Stump *et al.* 1986; Stump *et al.* 1991; Sircombe 1999). Instead, denudation of the Lachlan Fold Belt brought recycled Antarctic detritus as well as more juvenile (Silurian-Devonian) detritus to the Sydney Basin during the early-Late Permian (Sircombe 1999; Zaid & Al Gahtani 2015). Granitic suites of the Lachlan Fold Belt present Silurian-Devonian ages of (~417 Ma); correlating well with the Devonian peak seen in SY2014004 (Figure 6; Chappell *et al.* 1988). The broad array of age peaks seen in the U-Pb spectra of SY2014004 is unique, and does not appear in any of the following sediments within this study. The cause of such a provincial change is speculative, but (Moffitt 2000) has implied renewed uplift of the New England Fold Belt caused widespread pulses of detrital input into the basin, destabilizing, causing abrupt cycles of transgression, eroding detritus from the North and the West (Sircombe 1999).

Sequence stratigraphy of Permian Coal Measures in the Sydney Basin by Herbert (1995) shows a parasequence boundary shortly after deposition of the *Wilton Formation*.

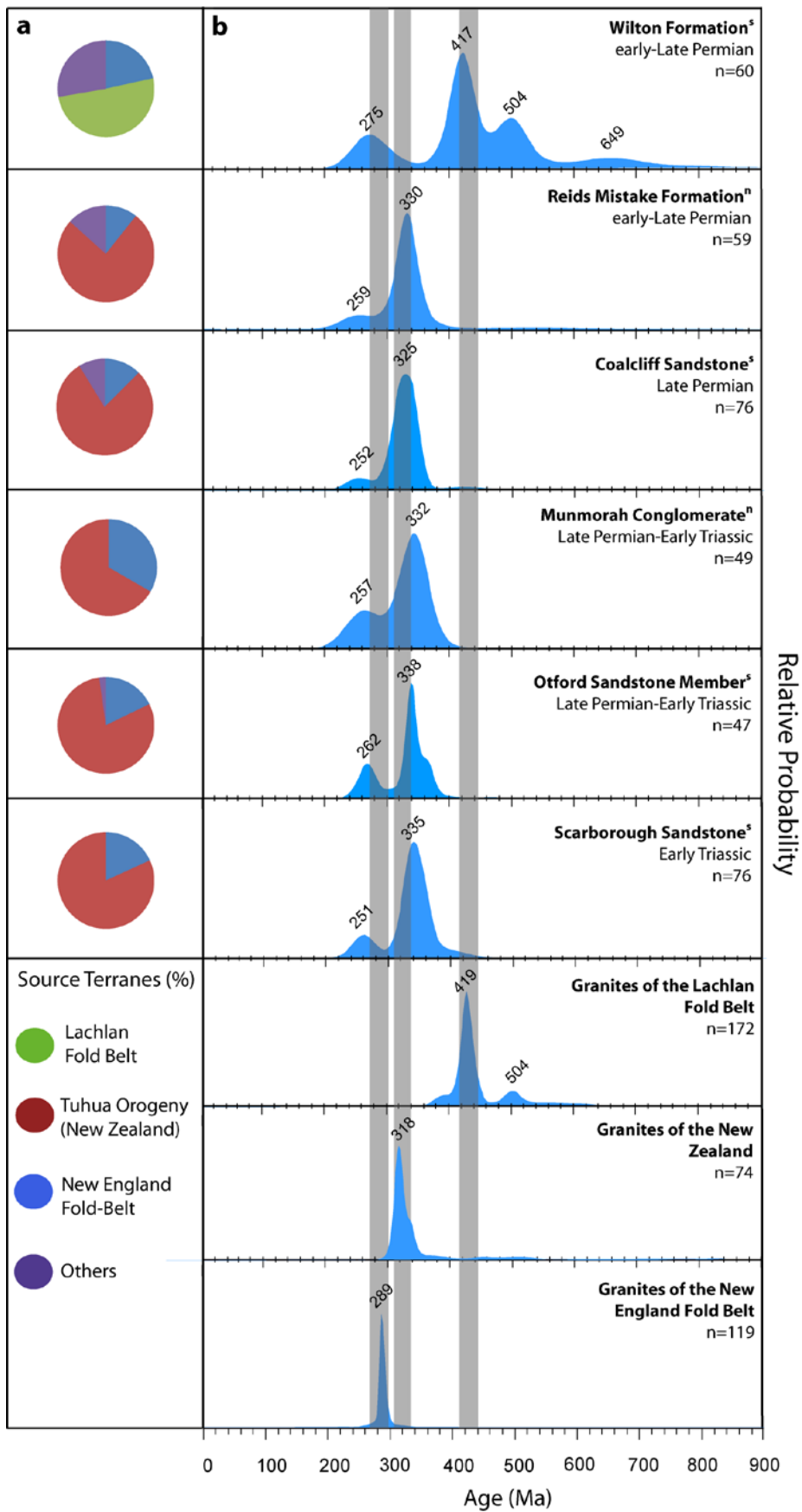


Figure 9: (a) Pie charts displaying the relative contribution of source terranes based on zircon age peaks (b) U-Pb age spectra of Sydney Basin samples coupled with U-Pb spectra of granites from source regions. Grey shaded areas correlate age peaks from source terranes with the U-Pb spectra of sediments from this study. Data for the Source Terrane Calculations and U-Pb spectra can be found in (Appendix A) All zircon data was filtered by a concordance threshold of >85%. New England Orogen data after Landenberger *et al.* (1995); Lachlan Fold Belt Data after Keay *et al.* (1999); New Zealand data after Tulloch *et al.* (2009b).

This parasequence boundary marks a shift from marine and deltaic sediments of the *Wilton Formation* to the deltaic and fluvial sediments of the *Reids Mistake Formation*.

This shift is a regional change, indicating both the north and south Sydney basins experienced a hiatus in marine influenced sedimentation in the Late Permian. The cessation of marine influence on sedimentation pre-determined the provenance and sedimentary pathway of all samples in this study after deposition of SY2014004, as can be seen in Figure 9a, where the relative input of provenance sources do not shift tremendously from SY2014004 onwards.

Provenance Constraints and Sediment Geomorphology at the P-T Boundary

The position of age peaks for South and North Sydney Basin sediments at the P-T Boundary; SY2014010 from the *Coalcliff Sandstone* and NS2014008 from the *Munmorah Conglomerate* correlate very well with each other. Figure 7 shows a Carboniferous peak of (~330 Ma) for both the *Coalcliff Sandstone* and *Munmorah Conglomerate* respectively. This Carboniferous peak as shown in Figure 9a is correlated with granitic suites of the New Zealand, emplaced during the Tuhua Orogeny (Gibson 1992). A second Permian peak (~255 Ma) is also present in both the South and North sediments at the P-T Boundary. This Permian peak as seen in Figure 9b is correlated with the uplift, exposure and erosion of granitic suites from the New England Fold Belt. The fundamental difference between the southern and northern sediments at the P-T boundary is the relative contribution of the Permian zircons. The *Munmorah*

Conglomerate contains a far higher relative contribution of Permian zircons than the *Coalcliff Sandstone*. This can be explained by the proximity of P-T boundary sediments to their source areas. The *Munmorah Conglomerate* in the north is located adjacent to the Hunter Mooki Thrust System, uplifting and eroding detritus from the New England Fold Belt (Collins 1991). By the time NEFB detrital material migrates to the southern margins of the Basin, intermingling with Carboniferous zircons occurs and the relative proportion of Carboniferous zircons to Permian zircons increases. The similarities in U-Pb spectra between the *Munmorah Conglomerate* and the *Coalcliff Sandstone* imply no provenance change occurred across the P-T boundary in the south or north Sydney Basin.

A difference in lithology however, between NS2014008 and SY2014010 does however imply palaeo-environmental change. In the north, uplift of the NEFB created steep slopes, generating alluvial fans responsible for the deposition of the *Munmorah Conglomerate* (Diessel 1992). This is contrasted to the meandering fluvial deposit of the *Coalcliff Sandstone* (Moffitt 2000). The *Coalcliff Sandstone* reflects the migration of meandering or anabranching rivers snaking across peaty wetlands in the Southern regions of the Basin (Davies 2015). Such a difference in deposition environment is due to the time-lag of the palaeo-environmental progradation from the north to the south (Dehghani 1994). Barren landscapes, devoid of vegetation after the mass extinction of deep-rooted vegetation around the P=T Boundary were dominant in the north. This theory is supported by the abundance coarse angular fragments found within the *Dooralong Shale* and *Munmorah Conglomerate* in the north Sydney Basin. In the south Sydney Basin, evidence of deep rooted vegetation is reflected in the fine grain nature of the *Coalcliff Sandstone*. It was not until after the deposition of the *Coalcliff Sandstone*

and the *Wombarra Claystone* in the south where the dominance of coarse grain sediments prevailed; resulting in the basin-wide deposition of the *Scarborough Sandstone*.

Provenance Constraints and Sediment Geomorphology into the Early Triassic

The position of age peaks in the south Sydney Basin sediments in the Early Triassic succession correlate well with each other. The U-Pb spectra for samples SY2014013 of the *Otford Sandstone Member* and SY2014014 of the *Scarborough Sandstone* display two age peaks (Figure 8); a Carboniferous (~335 Ma) and Permian (~258 Ma) peak. As stated above, the Carboniferous peak correlates with subsequent erosion of granites emplaced during the Tuhua Orogeny of New Zealand; the Permian peak is derived from granite sources within the New England Fold belt as seen in Figure 9b. The difference in U-Pb spectra seen within the Early Triassic succession of sediments in the south is the relative contributions of Carboniferous and Permian peaks. The *Otford Sandstone Member* (SY2014013) shows a lack of Early Carboniferous zircons compared to the *Scarborough Sandstone*. The *Otford Sandstone Member* however, has a greater contribution of Permian zircons than the *Scarborough Sandstone*. The decreased contribution of Permian zircons in the *Scarborough Sandstone* is attributed to the lack of sedimentary supply from the NEFB as tectonic activity ceased temporally in the Early Triassic (Moffitt 2000). The similarities in U-Pb spectra between the *Otford Sandstone Member* and the *Scarborough Sandstone* imply no provenance change occurred within the Early Triassic succession of the southern Sydney Basin sediments.

What did change was the fluvial morphology of the depositional systems in the Early-Triassic succession. The *Wombarra Claystone* represents a fine grain clay rich stratigraphy, deposited via a coupled meandering-estuary depositional system. An

abrupt facies change occurs with the deposition of the *Scarborough Sandstone*; a basin-wide erosional surface, where coarse sandstones with pebbly fragments dominate the stratigraphy (Dehghani 1994). Dehghani (1994) has also suggested the truncation of sediments in the north, particularly after deposition of the *Munmorah Conglomerate*, caused the progradation of alluvial fans and braid-plain palaeo-environments southwards. The generation of these barren landscapes were due to the disappearance of peat lands and deep rooted vegetation after the P-T Boundary, facilitating the collapse of fine grain terrestrial fluvial systems, where the river banks of meandering rivers collapsed and the stability of hill slopes readily decreased. Such a process increased sedimentation yield and was directly responsible for the truncation of sediments in the north, thus providing the necessary mechanism required for the progradation of this barren landscape southwards.

CONCLUSIONS

- Detrital zircon geochronology on Permian and Triassic sediments of the Sydney Basin reveals significant changes in detrital provenance near the P-T boundary. The zircon U-Pb results for early Late Permian sediments exhibit 4 distinct age peaks: Cambrian (~540-490 Ma); Silurian - Devonian (~440-390 Ma), Carboniferous (~360-300 Ma) and Permian - Triassic (~280-240 Ma). The latest Permian and Triassic sediments only yield two main age peaks; Carboniferous (~360-300 Ma) and Permian - Triassic (~280-240 Ma).

- In general, the provenance of Late Permian Sediment of the Sydney Basin can be attributed to an array of sources including the adjacent magmatic belt of the New England Orogen to the North, the Lachlan Fold Belt to the West, the Trans-Antartic Mountain Ranges to the South and the Tuhua Orogeny to the East.

- The broad array of 4 age peaks observed for the early Late Permian sediments of the southern Basin sediments can be attributed to favourable sediment pathways from all three tectonics sources, however, there is a noticeable absence of ~330 Ma zircons from the U-Pb age spectra. Deposition of the early-Late Permian Wilton Formation occurs before exposure of granitic bodies on the Western Province of New Zealand, which is thought to be largely responsible for an influx of Carboniferous detrital zircons immediately before the P-T boundary and into the Triassic. This influx of detrital material is represented by the ~330 Ma age peaks seen within all other sediments within this study (Figure 9b).
- This study suggests that the abrupt change in sedimentary provenance within the latest Permian is likely related with a tectonically induced paleo-environmental shift, restricting marine influence on sedimentation within the Sydney Basin.
- The succession of sediment - facies in early Triassic sediments from fine – coarse grain sediments without a provenance change imply a change in river morphology associated with the mass extinction of deep rooted vegetation after the P-T Boundary.

ACKNOWLEDGMENTS

I thank Stijn Glorie from the University of Adelaide for being a mentor and providing guidance. I would also like to thank Katie Howard for managing bookings and training for the ICP-MS, rock crushing room and mineral separation lab. I'd like to thank Ben Wade and Aoife McFadden for assistance on the New-Wave LA-ICPMS. A final thanks to Allan Collins, my Co-Supervisor for this project.

REFERENCES

- AITCHISON J., FLOOD P. & SPILLER F. 1992. Tectonic setting and paleoenvironment of terranes in the southern New England orogen, eastern Australia as constrained by radiolarian biostratigraphy. *Palaeogeography, Palaeoclimatology, Palaeoecology* **94**, 31-54.
- AITCHISON J. C. & BUCKMAN S. 2012. Accordion vs. quantum tectonics: Insights into continental growth processes from the Paleozoic of eastern Gondwana. *Gondwana Research* **22**, 674-680.
- ARDITTO P. 1991. A sequence stratigraphic analysis of the Late Permian succession in the southern coalfield, Sydney basin, New South Wales. *Australian Journal of Earth Sciences* **38**, 125-137.
- BENTON M. J. & NEWELL A. J. 2014. Impacts of global warming on Permo-Triassic terrestrial ecosystems. *Gondwana Research* **25**, 1308-1337.
- BRUNKER R. & ROSE G. 1969. *Sydney Basin Geological Map* (1st edition). Geological Survey of New South Wales, Sydney.
- CAS R., POWELL C. M. & CROOK K. 1980. Ordovician palaeogeography of the Lachlan Fold Belt: a modern analogue and tectonic constraints. *Journal of the Geological Society of Australia* **27**, 19-31.
- CAS R. A. 1983. *Special Publication*. Geological Society of Australia.
- CHAPPELL B., WHITE A. & HINE R. 1988. Granite provinces and basement terranes in the Lachlan Fold Belt, southeastern Australia. *Australian Journal of Earth Sciences* **35**, 505-521.
- COLLINS W. 1991. A reassessment of the 'Hunter-Bowen Orogeny': Tectonic implications for the southern New England fold belt. *Australian Journal of Earth Sciences* **38**, 409-423.
- COWAN E. J. 1993. Longitudinal fluvial drainage patterns within a foreland basin-fill: Permo-Triassic Sydney Basin, Australia. *Sedimentary geology* **85**, 557-577.
- CRAPP C. & NOLAN R. 1975. Economic Geology of Australia and Papua New Guinea. 2. Coal, Australasian Institute of Mining Metallurgy, Melbourne. *Monograph Series*, 163-175.
- DAVIES N. 2015. Final Report on Project GEFNE94-13 for National Geographic Society's Global Exploration Fund - Northern Europe. *National Geographic*.
- DEHGHANI M. H. 1994. Sedimentology, genetic stratigraphy and depositional environment of the Permo-Triassic succession in the Southern Sydney Basin, Australia.
- DIESSEL C. F. K. 1992. *Coal-bearing depositional systems* (1st edition). Springer-Verlag, Berlin & Heidelberg.
- DRAGOVICH D. & PATTERSON J. 1995. Condition of rehabilitated coal mines in the Hunter Valley, Australia. *Land Degradation & Development* **6**, 29-39.
- FEDERICO L., CRISPINI L., CAPPONI G. & BRADSHAW J. 2009. The Cambrian Ross Orogeny in northern Victoria Land (Antarctica) and New Zealand: a synthesis. *Gondwana Research* **15**, 188-196.
- FLOOD R. & SHAW S. 1977. Two "S-type" granite suites with low initial $^{87}\text{Sr}/^{86}\text{Sr}$ ratios from the New England Batholith, Australia. *Contributions to Mineralogy and Petrology* **61**, 163-173.

- FOSTER D. A. & GRAY D. R. 2000. Evolution and structure of the Lachlan Fold Belt (Orogen) of eastern Australia. *Annual Review of Earth and Planetary Sciences* **28**, 47-80.
- GIBSON G. 1992. Medium-high-pressure metamorphic rocks of the Tuhua Orogen, western New Zealand, as lower crustal analogues of the Lachlan Fold Belt, SE Australia. *Tectonophysics* **214**, 145-157.
- GLEN R. & BECKETT J. 1997. Structure and tectonics along the inner edge of a foreland basin: the Hunter Coalfield in the northern Sydney Basin, New South Wales. *Australian Journal of Earth Sciences* **44**, 853-877.
- GOODGE J., MYROW P., WILLIAMS I. & BOWRING S. 2002. Age and provenance of the Beardmore Group, Antarctica: constraints on Rodinia supercontinent breakup. *The Journal of geology* **110**, 393-406.
- GOSTIN V. & HERBERT C. 1973. Stratigraphy of the upper Carboniferous and lower Permian sequence, southern Sydney Basin. *Journal of the Geological Society of Australia* **20**, 49-70.
- GRAY D. R. 1997. Tectonics of the southeastern Australian Lachlan Fold Belt: structural and thermal aspects. *Geological Society, London, Special Publications* **121**, 149-177.
- GRAY D. R. & FOSTER D. A. 1997. Orogenic concepts; application and definition; Lachlan fold belt, eastern Australia. *American Journal of Science* **297**, 859-891.
- GREEN D. 1973. Radiometric evidence of the Kanimblan Orogeny in southeastern Queensland and the age of the Neranleigh-Fernvale Group. *Journal of the Geological Society of Australia* **20**, 153-160.
- GREEN R. & KRIDOHARTO P. 1975. New evidence on the form of the granitic intrusions in new England, NSW. *Journal of the Geological Society of Australia* **22**, 51-59.
- GRINDLEY G. & MCDUGALL I. 1969. Age and correlation of the Nimrod Group and other Precambrian rock units in the central Transantarctic Mountains, Antarctica. *New Zealand Journal of Geology and Geophysics* **12**, 391-411.
- GULSON B., DIESSEL C., MASON D. & KROGH T. 1990. High precision radiometric ages from the northern Sydney Basin and their implication for the Permian time interval and sedimentation rates. *Australian Journal of Earth Sciences* **37**, 459-469.
- HAMILTON D. 1991. Genetic stratigraphy of the Gunnedah Basin, NSW. *Australian Journal of Earth Sciences* **38**, 95-113.
- HAMILTON D. S. & TADROS N. 1994. Utility of coal seams as genetic stratigraphic sequence boundaries in nonmarine basins: an example from the Gunnedah Basin, Australia. *AAPG bulletin* **78**, 267-286.
- HERBERT C. 1995. Sequence stratigraphy of the Late Permian coal measures in the Sydney Basin. *Australian Journal of Earth Sciences* **42**, 391-405.
- HERBERT C. & HELBY R. 1980. *A guide to the Sydney Basin*. D. West, Govt. Printer.
- HOLCOMBE R., STEPHENS C., FIELDING C., GUST D., LITTLE T., SLIWA R., KASSAN J., MCPHIE J. & EWART A. 1997. Tectonic evolution of the northern New England Fold Belt: the Permian-Triassic Hunter-Bowen event. *Tectonics and metallogenesis of the New England Orogen* **19**, 52-65.

- HUNT J. W. 1988. Sedimentation rates and coal formation in the Permian basins of eastern Australia. *Journal of the Geological Society of Australia* **35**, 259-274.
- HUTTON A. & BAMBERRY J. 1999. Stratigraphy and terminology for the Southern Coalfield. *Coalfield Geol Counc NSW Bull* **1**, 120-152.
- HUTTON A. C. 2009. Geological setting of australasian coal deposits.
- JACKSON S. E., PEARSON N. J., GRIFFIN W. L. & BELOUSOVA E. A. 2004. The application of laser ablation-inductively coupled plasma-mass spectrometry to in situ U–Pb zircon geochronology. *Chemical geology* **211**, 47-69.
- JAKEMAN B. 1980. The relationship between formation structure and thickness in the Permo-Triassic succession of the Southern Coalfield, Sydney Basin, New South Wales, Australia. *Journal of the International Association for Mathematical Geology* **12**, 185-212.
- JONES J., CONAGHAN P., MCDONNELL K., FLOOD R. & SHAW S. 1984. Papuan Basin analogue and a foreland basin model for the Bowen-Sydney Basin. *Phanerozoic earth history of Australia*, 243-262.
- KEAY S., STEELE D. & COMPSTON W. 1999. Identifying granite sources by SHRIMP U-Pb zircon geochronology: An application to the Lachlan foldbelt. *Contributions to Mineralogy and Petrology* **137**, 323-341.
- LAIRD M. G. 1991. The Late Proterozoic-Middle Palaeozoic rocks of Antarctica. *The Geology of Antarctica*. Clarendon Press, Oxford, 74-119.
- LANDENBERGER B., FARRELL T. R., OFFLER R., COLLINS W. J. & WHITFORD D. J. 1995. Tectonic implications of Rb–Sr biotite ages for the Hillgrove Plutonic Suite, New England Fold Belt, N.S.W., Australia. *Precambrian Research* **71**, 251-263.
- LEITCH E. 1975. Plate tectonic interpretation of the Paleozoic history of the New England Fold Belt. *Geological Society of America Bulletin* **86**, 141-144.
- LOVERING J. F. 1953. *The stratigraphy of the Wianamatta Group, Triassic System, Sydney Basin*. University of Sydney.
- LUDWIG K. 2012. User's Manual For Isoplot 3.75. A Geochronological Toolkit for Microsoft Excel. Berkeley Geochronology Center Special Publication.
- MENSEL H., MCCULLOCH M. & CHAPPELL B. 1985. The New England Batholith: constraints on its derivation from Nd and Sr isotopic studies of granitoids and country rocks. *Geochimica et Cosmochimica Acta* **49**, 369-384.
- MOFFITT R. 2000. Appendix A, Geological Setting.
- MURRAY C., FERGUSON C., FLOOD P., WHITAKER W. & KORSCH R. 1987. Plate tectonic model for the Carboniferous evolution of the New England Fold Belt. *Australian Journal of Earth Sciences* **34**, 213-236.
- NEUFELD L. M. Introduction to Laser Ablation ICP-MS for the Analysis of Forensic Samples.
- OFFLER R. & GAMBLE J. 2002. Evolution of an intra-oceanic island arc during the Late Silurian to Late Devonian, New England Fold Belt*. *Australian Journal of Earth Sciences* **49**, 349-366.
- PANKHURST R., STOREY B., MILLAR I., MACDONALD D. & VENNUM W. 1988. Cambrian-Ordovician magmatism in the Thiel Mountains, Transantarctic Mountains, and implications for the Beardmore orogeny. *Geology* **16**, 246-249.
- PAYNE J. L., PEARSON N. J., GRANT K. J. & HALVERSON G. P. 2013. Reassessment of relative oxide formation rates and molecular interferences on in situ lutetium–

- hafnium analysis with laser ablation MC-ICP-MS. *Journal of Analytical Atomic Spectrometry* **28**, 1068-1079.
- RETALLACK G. J. 1999. Postapocalyptic greenhouse paleoclimate revealed by earliest Triassic paleosols in the Sydney Basin, Australia. *Geological Society of America Bulletin* **111**, 52-70.
- RETALLACK G. J., VEEVERS J. J. & MORANTE R. 1996. Global coal gap between Permian–Triassic extinction and Middle Triassic recovery of peat-forming plants. *Geological Society of America Bulletin* **108**, 195-207.
- ROGERS J. J. 1993. *A History of the Earth*. CUP Archive.
- RUST B. R. & JONES B. G. 1987. The Hawkesbury Sandstone south of Sydney, Australia: Triassic analogue for the deposit of a large, braided river. *Journal of Sedimentary Research* **57**.
- SCHEIBNER E. 1973. A plate tectonic model of the Palaeozoic tectonic history of New South Wales. *Journal of the Geological Society of Australia* **20**, 405-426.
- SCOTT J., MUHLING J., FLETCHER I., BILLIA M., PALIN J. M., ELLIOT T. & GÜNTER C. 2011. The relationship of Palaeozoic metamorphism and S-type magmatism on the paleo-Pacific Gondwana margin. *Lithos* **127**, 522-534.
- SHAW S. & FLOOD R. 1981. The New England Batholith, eastern Australia: geochemical variations in time and space. *Journal of Geophysical Research: Solid Earth (1978–2012)* **86**, 10530-10544.
- SHI G. R. & MCLOUGHLIN S. 1997. *Permian Stratigraphy, Sedimentology and Palaeontology of the Southern Sydney Basin, Eastern Australia: A Field Excursion Guide*. School of Aquatic Science and Natural Resources Management, Deakin University.
- SIRCOMBE K. N. 1999. Tracing provenance through the isotope ages of littoral and sedimentary detrital zircon, eastern Australia. *Sedimentary geology* **124**, 47-67.
- SLÁMA J., KOŠLER J., CONDON D. J., CROWLEY J. L., GERDES A., HANCHAR J. M., HORSTWOOD M. S., MORRIS G. A., NASDALA L. & NORBERG N. 2008. Plešovice zircon—a new natural reference material for U–Pb and Hf isotopic microanalysis. *Chemical geology* **249**, 1-35.
- STUMP E., KORSCH R. & EDGERTON D. 1991. The myth of the Nimrod and Beardmore orogenies. *Geological Evolution of Antarctica*. Cambridge University Press, Cambridge, 143-147.
- STUMP E., SMIT J. & SELF S. 1986. Timing of events during the late Proterozoic Beardmore Orogeny, Antarctica: geological evidence from the La Gorce Mountains. *Geological Society of America Bulletin* **97**, 953-965.
- TULLOCH A. J., RAMEZANI J., MORTIMER N., MORTENSEN J., VAN DEN BOGAARD P. & MAAS P. 2009a. *Cretaceous felsic volcanism in New Zealand and Lord Howe Rise (Zealandia) as a precursor to final Gondwana break-up*. *Geological Society Special Publication*. **321**: 89-118.
- TULLOCH A. J., RAMEZANI J., MORTIMER N., MORTENSEN J., VAN DEN BOGAARD P. & MAAS P. 2009b. *Cretaceous felsic volcanism in New Zealand and Lord Howe Rise (Zealandia) as a precursor to final Gondwana break-up*. *Geological Society Special Publication*. **321**: 89-118.

- TYE S., FIELDING C. & JONES B. 1996. Stratigraphy and sedimentology of the Permian Talaterang and Shoalhaven groups in the southernmost Sydney Basin, New South Wales. *Australian Journal of Earth Sciences* **43**, 57-69.
- VEEVERS J. 2003. Pan-African is Pan-Gondwanaland: oblique convergence drives rotation during 650–500 Ma assembly. *Geology* **31**, 501-504.
- VEEVERS J., CONAGHAN P. & SHAW S. 1993. Permian and Triassic New England Orogen/Bowen–Gunnedah–Sydney Basin in the context of Gondwanaland and Pangea. *New England Orogen, eastern Australia*, 31-51.
- VEEVERS J. J. & MORGAN P. 2000. *Billion-year earth history of Australia and neighbours in Gondwanaland*. Gemoc Press.
- VERMEESCH P. 2012. On the visualisation of detrital age distributions. *Chemical geology* **312**, 190-194.
- WADE B., HAND M., MAIDMENT D., CLOSE D. & SCRIMGEOUR I. 2008. Origin of metasedimentary and igneous rocks from the Entia Dome, eastern Arunta region, central Australia: a U–Pb LA-ICPMS, SHRIMP and Sm–Nd isotope study. *Australian Journal of Earth Sciences* **55**, 703-719.
- WADIA A. M. 2015. Silica Enrichment in a Volcanic Setting Using Petrographic Analyses and Mass Balance Calculations Using Trace Element Zircon. *Journal of Geological Resource and Engineering* **2**, 108-117.
- WARD C. R. 1972. Sedimentation in the Narrabeen Group, southern Sydney Basin, New South Wales. *Journal of the Geological Society of Australia* **19**, 393-409.
- WARD P. D., MONTGOMERY D. R. & SMITH R. 2000. Altered river morphology in South Africa related to the Permian-Triassic extinction. *Science* **289**, 1740-1743.
- WATANABE T., IWASAKI M., ISHIGA H., ILIZUMI S., HONMA H., KAWACHI Y., MORRIS P., NAKA T. & ITAYA T. 1988. Late Carboniferous orogeny in the southern New England fold belt, NSW, Australia. *The New England Orogen: Tectonics and Metallogenesis*, 93-98.
- WIGHTMAN W. G., SCOTT D. B., MEDIOLI F. S. & GIBLING M. R. 1994. Agglutinated foraminifera and thecamoebians from the Late Carboniferous Sydney coalfield, Nova Scotia: paleoecology, paleoenvironments and paleogeographical implications. *Palaeogeography, Palaeoclimatology, Palaeoecology* **106**, 187-202.
- WILLIAMS I., CHAPPELL B., CROOK K. & NICOLL R. 1994. In search of the provenance of the early Palaeozoic flysch in the Lachlan Fold Belt, southeastern Australia. *Geological Society of Australia Abstracts*, p. 464.
- WILLIAMS I. S. 1992. Some observations on the use of zircon U-Pb geochronology in the study of granitic rocks. *Transactions of the Royal Society of Edinburgh: Earth Sciences* **83**, 447-458.
- ZAID S. M. & AL GAHTANI F. 2015. Provenance, diagenesis, tectonic setting, and geochemistry of Hawkesbury Sandstone (Middle Triassic), southern Sydney Basin, Australia. *Turkish Journal of Earth Sciences* **24**, 72-98.

APPENDIX A:

Methods

ROCK CRUSHING AND MINERAL SEPARATION

Entering the lab, the floor of the rock crushing room is vacuumed as well as all floors and benches including inside the fumigator and the sink. They were then cleaned with paper towel and ethanol to minimize contamination from other sediments. The Frantz machine was then pulled apart and cleaned with compressed air, followed by the cleaning of the sink with ethanol and inside the heavy liquids fumigator with acetone. All fine grains had to be removed before the sample could even be taken out. After this both panning bowls were thoroughly cleaned with ethanol and water and left to dry, as well as the two plastic beakers and funnels used for sediment collection. Once the lab was completely sterilised the sample was placed in the small panning bowl and filled with water. The bowl was carefully shaken to remove fine dirt particles within the sediment. The larger panning bowl was placed underneath to collect water that ran off, as all sediment had to be retained if the need for more zircons was crucial. This process was all done slowly and carefully, taking about 20 minutes to 40 minutes per sample, making sure no sediment-containing water was flowing down the sink. When all the dirt particles were removed and the water was less murky, the small pan bowl was placed to the side and the larger pan bowl was removed from the sink, and poured into filter paper in each of the two funnels located next to the sink. These filters slowly removed water from the sample that collected in the large pan bowl. From this stage, the large pan bowl was placed underneath the small pan bowl again and filled with clean water. The small pan bowl was also filled with water and tilted on angle, held carefully and slowly shaken such that the sediment at the bottom of the bowl did not move but the water above 'sloshed' around. This was to promote the sinking of heavy minerals like zircon so that the lighter minerals and dirt could be drawn off. This process was very lengthy and took anywhere from 30 minutes to 2 hours per sample, to pan down to a tiny fraction of sediment. This process is done in the hopes of concentrating zircons down the very bottom of the sample. When shaking of the small pan bowl occurs, every 20 seconds or so the bowl is pushed into the larger pan bowl below still at the same angle, and drawn back out. This is so the light minerals and the bulk of sediment could flow out of the small pan bowl into the large pan bowl to concentrate zircons in the small pan bowl. This process occurred until the sample was reduced to the size of a 20c coin (approximately). When this process was finalised, the remaining zircon fraction was poured into a small filter inside a small funnel on top of a conical flask and left to filter out water. When this process was complete the filter paper with sample inside was removed and placed on the hot plate to just over 120 degrees. A funnel was placed on top of the sample to promote the evaporation of water from the sample to prepare the sample for magnetic mineral separation. This drying process on average took about 30 minutes. Once the sample was completely dry it was taken over to the Franz machine, where the sample was poured into a funnel, flowing into a test tube with a hole at the bottom. The Frantz machine was turned on and set to 0.5Amps. A finger was placed over the test tube hole and slowly removed to allow the slow pouring of sediment onto the Frantz machine where magnetic minerals were separated from non-magnetic

minerals. Once all the sediment fraction was split, the magnetics were bagged up and labelled and the non-magnetic fraction was sent through the machine again at 1 Amp. After completion the magnetics were labelled in a separate bag and labelled, and the non-magnetic fraction went through again at 1.5 Amps. The magnetic fraction was again bagged and labelled and the non-magnetic fraction was brought over to the heavy liquids area. The Frantz machine was then dismantled and cleaned with compressed air to prevent contamination for future samples. Running through the Frantz three times allows for ideal separation of magnetic minerals from the original sample concentrating zircons in the non-magnetic fraction.

Meanwhile the large filter papers used at the start of the session were sprayed with ethanol to promote the seepage of water from the sample and to assist in drying out. Once dry the filter paper containing sample was removed from the funnel and labelled, placed into a bowl which in turn was placed in the oven over night to dry out completely, ready for future analysis if required.

At the heavy liquids station an apparatus was set up involving multiple beakers, a valve, filter paper and a bottle of iodine. The funnels were set up such that the first top funnel flows into the next bubble chamber containing a valve, which flows into another funnel with filter paper which flows into the bottle of iodine. This is to recycle the iodine. Zircons collect in the middle funnel inside filter paper. The top funnel is filled with iodine and filtered through filter paper to collect in the second bubble chamber which is sealed by the closed valve. Once enough iodine has been filtered through the top funnel is removed and the non-magnetic fraction of sediment is poured into the bubble chamber. The chamber is given a quick stir with a stirring rod and left to settle. The idea here is that light minerals float and heavy minerals including zircons sink to the bottom. When no more sediment is sinking the valve is opened, dropping zircons into the second funnel/filter paper. The bubble chamber is given another stir and left to settle until no more minerals are sinking. This process is repeated multiple times of the course of an hour and a half to maximise the concentration of zircons down the bottom of the of the bubble chamber. Once completed the filter paper containing the sample is removed and placed on the hot plate to dry at 120 degrees and then placed into a vial and labelled. Going back over to the apparatus, the result of solution is poured into the middle funnel with a new filter paper to collect the light minerals. Once filtered through this sample was placed onto the hot plate to dry before analysed under an Olympus SZ51 light microscope for the presence of zircons. If >100 zircons were present, the sample was placed in a vial for mounting. If there was few to no zircons present, the process of panning, magnetic mineral separation and heavy liquids were repeated until enough zircons were present. The apparatus was then thoroughly cleaned with acetone ten times before being placed on clean paper towel to dry. The lab was then cleaned again with ethanol and paper towel and vacuumed. This process was repeated to complete mineral separation for all six samples. Plastic gloves, a lab coat and safety glasses were used for the handling of heavy liquids.

ZIRCON MOUNTING

The zircon concentrate from the mineral separation procedure was poured into a petri dish and under an Olympus SZ51 light microscope. A separate glass slide containing a layer of adhesive taped was used to mount lines of zircons. A single piece of double sided tape was placed on top of the glass slide, ensuring no air bubbles developed. A

single piece of adhesive tape was then placed on top of the double sided tape, adhesive side upwards also ensuring no air bubbles developed. A rubber mould used for creating resin mounts (discussed below) was used to measure the boundaries of each line of zircons to ensure they fit well within the boundaries of the mount. Approximately 250 zircons per sample were mounted on two lines on the glass slide. 3 samples were mounted per slide, totalling 6 lines. Each line was engraved into the double side tape using a sharp blade. Then, Using a pick, zircons were selected from the petri dish and placed into the mount; this process repeated until all 6 samples were mounted. When all zircons had been mounted, the rubber moulds were placed over the zircon slides, ensuring each zircon line fits within the boundaries of the rubber mould. Then, a mix of epoxy resin 20-8130-032 and epoxy hardener 20-8132-008 (5 parts resin, 1 part hardener) was mixed thoroughly with a wooden stick. This epoxy mix was poured into each rubber mount up to a depth of 1 cm. A small sliver of paper with sample names was placed into the resin inside the rubber mount and set to dry for 24 hours. Once set the glass slide was removed as the zircons have now been engraved onto the set epoxy resin. Any remaining sticky tape was removed. The surfaces of each mount (2 mounts) were then ground down and polished using sand belts of varying thickness starting from 400 µm. For the thicker sand belts, the slides were manually ground down. For the final stage of polishing, diamond paste was rubbed into the zircon mounts and placed on the Struers DP-U4 cloth lap and left for 20 mins until all zircon surfaces had been exposed. Each sample was then taken to Adelaide Microscopy at the University of Adelaide to be carbon coated.

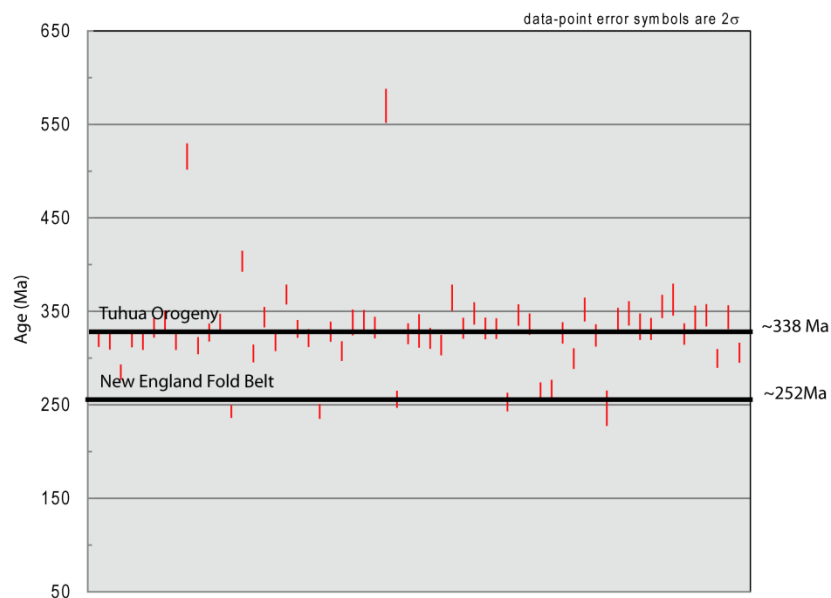
LA-ICP-MS AND GEOCHRONOLOGY

U-Pb zircon geochronology was conducted on six samples from the Sydney Basin. The Carbon coat from each zircon slide was removed. Laser-Ablation Inductively Coupled Plasma Mass Spectrometry (LA-ICP-MS) was performed using a New-Wave UP-213 laser attached to an Agilent 7500cx (ICP-MS). This equipment was accessed at Adelaide Microscopy at the University of Adelaide. Laser Ablation was carried out on each zircon mount, located in a sealed chamber within the New Wave laser UP-213 laser. The chamber is purged of any excess gas and material three times before the Helium count is turned up. Once the helium count is stable, the plasma on the ICP-MS is ignited, with the machine taking around 5 minutes to calibrate. Once the ICP-MS was set from 'standby' to 'ready' than grains could begin to be selected through the New Wave software for laser ablation. A laser frequency of 5 Hz and a fluence of 7J/cm² was selected for a spot size of 30 µm. A washout delay of 20 seconds and a dwell time of 30 seconds was selected for the laser as to ensure the laser and ICP-MS work effectively together. Isotopes ratios measured through LA-ICP-MS were ²⁰⁶Pb/²⁰⁷Pb, ²⁰⁶Pb/²³⁸U and ²⁰⁷Pb/²³⁵U. Absolute standard errors were provided with both isotope ratios and age estimates. Age corrections were performed on each sample using the Glitter software, using the zircon standard GJ-1 and a standard checker the Plešovice zircon (Jackson *et al.* 2004). An overestimated uncertainty of 1% was applied to the TIMS derived normalisation age-data for GJ-1, after (Jackson *et al.* 2004). Instrument drift was also corrected using the GLITTER software, bracketing every 20 unknown samples by performing 5 analyses checks on GJ-1, 3 on Plešovice and another on GJ-1 respectively. Age estimates produced via LA-ICP-MS on the Plešovice are checked with 1% uncertainty ages for the Plešovice sample from (Sláma *et al.* 2008) to attain

greater precision. Due to the unresolvable ^{204}Hg on ^{205}Pb interference, Concordia plots generated using Isoplot 3.75 (Ludwig 2012) do not display Discordia curves correcting for common lead. $^{206}\text{Pb}/^{238}\text{U}$ age estimates were used for ages <1 Ga and $^{207}\text{Pb}/\text{Pb}$ age estimates were used for ages >1 Ga. Weighted averages were produced using Isoplot with 2σ confidence values utilised. U-Pb frequency distribution diagrams with kernel density estimate curves were produced using Peter Vermeesch's software "Density Plotter (Vermeesch 2012)." Diagrams were produced using Adobe Illustrator 8 and Adobe Illustrator CS2.

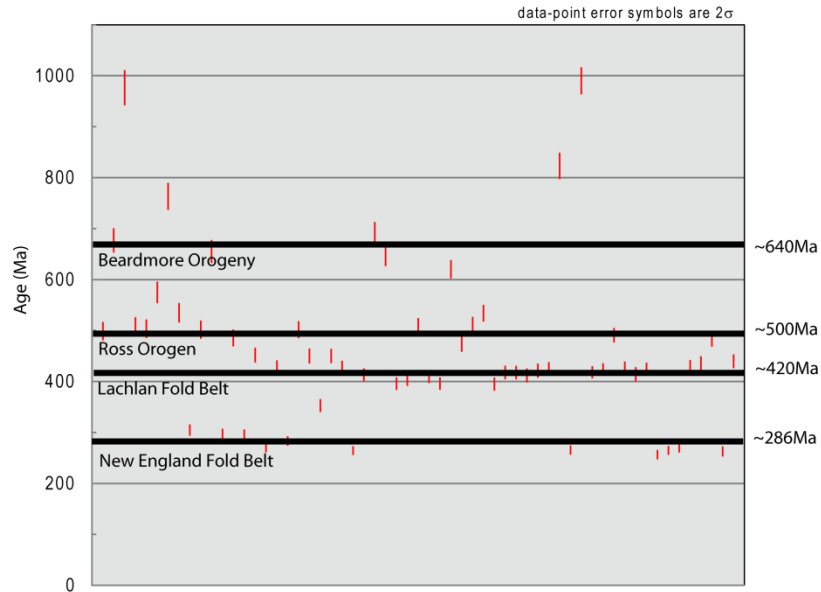
Weighted Averages for Provenance Pie Charts

NS2014002 – REIDS MISTAKE FORMATION



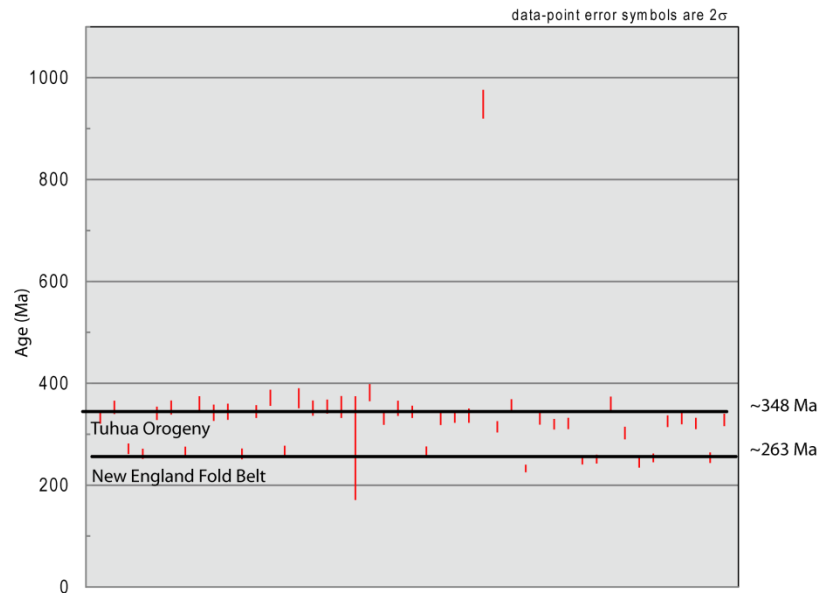
Supplementary Figure 1. Weighted Average Plots of U-Pb ages using the $\text{Pb}^{206}/\text{U}^{238}$ age estimates and standard errors (absolute). Bold lines indicate the weighted average of age estimates that correspond to age peaks of the U-Pb Age Spectra (Figs. 6-8). Weighted averages were used to construct pie charts of relative provenance contribution (Fig. 9). Plots were constructed using Isoplot, after (Ludwig 2012). Weighted average plots of detrital zircons from sample NS2014002 of the early-Late Permian Reids Mistake Formation.

SY2014004 – WILTON FORMATION



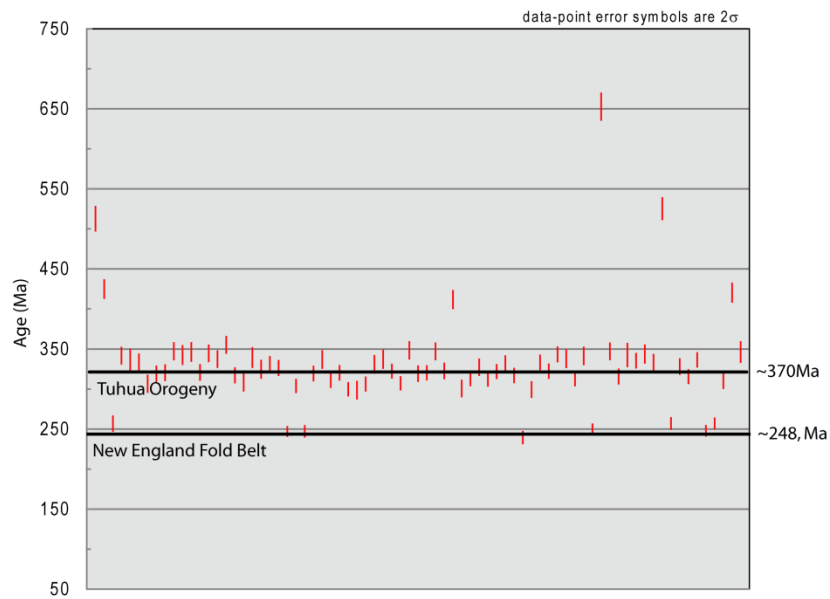
Supplementary Figure 2. Weighted average plots of detrital zircons from sample SY2014004 of the early-Late Permian Wilton Formation (see caption for Supplementary Figure 1) Note: Beardmore and Ross Orogens were incorporated into ‘others’ on the pie chart seen in figure 9a.

NS2014008 – MUNMORAH CONGLOMERATE



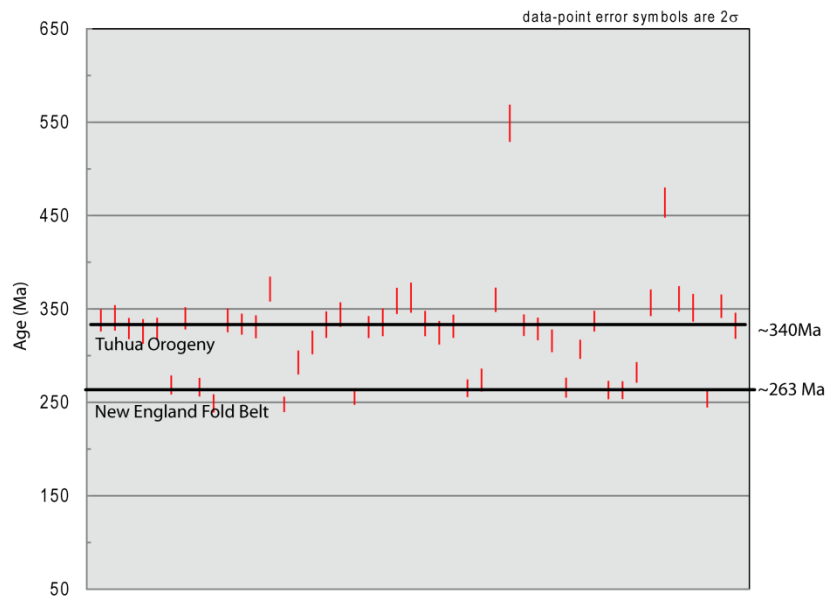
Supplementary Figure 3. Weighted average plots of detrital zircons from sample NS2014008 of the Late Permian-Early Triassic Munmorah Conglomerate (see caption for Supplementary Figure 1).

SY2014010 – COALCLIFF SANDSTONE



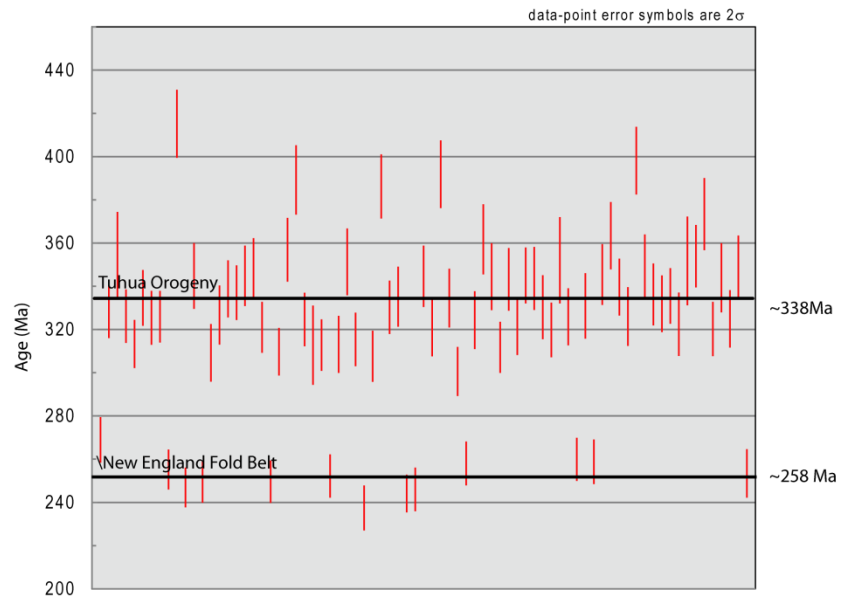
Supplementary Figure 4: Weighted average plots of detrital zircons from sample SY2014010 of the Late Permian Coalcliff Sandstone (see caption for Supplementary Figure 1).

SY2014013 – OTFORD SANDSTONE MEMBER



Supplementary Figure 5: . Weighted average plots of detrital zircons from sample SY2014010 of the Late Permian Coalcliff Sandstone (see caption for Supplementary Figure 1).

SY2014014 – SCARBOROUGH SANDSTONE



Supplementary Figure 6: Weighted average plots of detrital zircons from sample SY2014014 of the Early Triassic Scarborough Sandstone (see caption for Supplementary Figure 1).

2

Stratigraphic Formation

$^{206}\text{Pb}/^{207}\text{Pb}$	$^{206}\text{Pb}/^{207}\text{Pb}$	$^{206}\text{Pb}/^{238}\text{U}$	$^{206}\text{Pb}/^{238}\text{U}$	$^{207}\text{Pb}/^{235}\text{U}$	$^{207}\text{Pb}/^{235}\text{U}$	$^{207}\text{Pb}/^{206}\text{Pb}$	$^{207}\text{Pb}/^{206}\text{Pb}$	$^{206}\text{Pb}/^{238}\text{U}$	$^{206}\text{Pb}/^{238}\text{U}$	$^{207}\text{Pb}/^{235}\text{U}$	$^{207}\text{Pb}/^{235}\text{U}$	Rho	Con
1σ	1σ	1σ	1σ	1σ	1σ	Age (Ma)	1σ	Age (Ma)	1σ	Age (Ma)	1σ		
0882	0.01073	0.05203	0.00165	0.77958	0.0739	1779.8	169.86	327	10.1	585.2	42.16	0.04476004	
9525	0.00453	0.05368	0.00108	0.70406	0.03213	1533.1	86.88	337.1	6.59	541.2	19.14	0.122802471	
0729	0.00314	0.05347	0.00094	0.53667	0.02252	1011.1	84.83	335.8	5.76	436.2	14.88	0.145483666	
5713	0.00142	0.05106	0.00074	0.40168	0.01006	496	54.55	321	4.51	342.9	7.29	0.302343255	
5462	0.00132	0.05057	0.00072	0.38035	0.00926	396.7	52.87	318	4.42	327.3	6.81	0.304930916	
5779	0.00154	0.04521	0.00066	0.35974	0.00958	521.5	57.57	285	4.08	312	7.15	0.272871817	
7365	0.00306	0.05433	0.00096	0.55104	0.02233	1031.8	81.83	341.1	5.84	445.7	14.62	0.159307306	
7146	0.004	0.05413	0.00106	0.53271	0.02911	970.7	110.27	339.8	6.47	433.6	19.28	0.110421087	
9316	0.00605	0.04953	0.00115	0.63551	0.03977	1491.2	118.12	311.6	7.03	499.5	24.69	0.081842655	
5904	0.00154	0.051	0.00075	0.41469	0.01086	568.6	55.94	320.7	4.58	352.2	7.8	0.287845943	
8012	0.00342	0.05279	0.00097	0.58257	0.02411	1200	81.78	331.6	5.93	466.1	15.47	0.150111504	
0549	0.0011	0.05046	0.0007	0.38152	0.00788	408	43.92	317.3	4.27	328.2	5.79	0.379692303	
0899	0.0019	0.04041	0.00057	0.60665	0.01094	1782.5	31.56	255.4	3.51	481.4	6.92	0.43296532	
5706	0.00205	0.0529	0.00084	0.41579	0.01479	493.2	78.07	332.3	5.17	353	10.6	0.2006549	
6126	0.0019	0.05423	0.00084	0.45762	0.01404	648.3	65.13	340.4	5.12	382.6	9.78	0.230696994	
1745	0.00181	0.04343	0.00059	0.7026	0.01153	1917.8	27.41	274	3.66	540.3	6.88	0.48525891	
8363	0.00135	0.04846	0.00066	0.55831	0.0096	1283.7	31.29	305.1	4.05	450.4	6.26	0.470930318	
0687	0.00146	0.0511	0.00073	0.48355	0.01048	889.6	43.34	321.2	4.47	400.5	7.17	0.358772458	
5384	0.00118	0.0505	0.00071	0.37456	0.00841	364.3	48.87	317.6	4.37	323	6.21	0.350769324	
5598	0.00143	0.03835	0.00056	0.29575	0.00763	451.1	55.82	242.6	3.47	263.1	5.98	0.300311619	
5824	0.00115	0.08327	0.00117	0.6684	0.01372	538.3	43.19	515.6	6.95	519.7	8.35	0.396764923	
5516	0.00146	0.04981	0.00074	0.37864	0.01011	418.5	57.57	313.3	4.54	326	7.45	0.293775033	
6738	0.00278	0.05503	0.00096	0.51105	0.02067	849.5	83.47	345.3	5.85	419.2	13.89	0.168621093	
7533	0.0034	0.05066	0.00094	0.52608	0.02309	1077.4	87.91	318.6	5.78	429.2	15.37	0.143380296	
8498	0.00489	0.05267	0.00112	0.61694	0.03441	1315.1	107.74	330.9	6.87	487.9	21.61	0.106181093	
7603	0.00148	0.07184	0.00102	0.75287	0.01526	1095.8	38.52	447.2	6.16	569.9	8.84	0.40568596	
5225	0.00148	0.0521	0.00078	0.37523	0.01065	296.4	63.06	327.4	4.8	323.5	7.86	0.267558315	
0606	0.00107	0.05386	0.00075	0.44994	0.00849	625.2	37.78	338.2	4.56	377.2	5.94	0.453258133	
5887	0.00114	0.0384	0.00054	0.31162	0.00632	562.2	41.64	242.9	3.35	275.4	4.89	0.410384195	
5556	0.00118	0.0646	0.00092	0.49485	0.01085	434.6	46.05	403.6	5.58	408.2	7.37	0.372284958	
6293	0.00199	0.04843	0.00077	0.42019	0.01324	705.7	66.04	304.9	4.73	356.2	9.46	0.245179713	
0666	0.00275	0.04928	0.00086	0.45247	0.01835	825.2	83.92	310.1	5.3	379	12.83	0.172591023	
5795	0.002	0.05478	0.00088	0.43764	0.01497	527.4	74.13	343.8	5.4	368.6	10.57	0.215661594	
6252	0.0022	0.05053	0.00083	0.4356	0.01519	692.1	73.45	317.8	5.1	367.1	10.74	0.216115771	
6379	0.0015	0.05875	0.00087	0.51677	0.01241	734.7	49.09	368	5.29	423	8.31	0.341729582	
0937	0.0045	0.04596	0.00093	0.59387	0.02753	1502.1	88.1	289.7	5.72	473.3	17.54	0.134303302	
5327	0.0013	0.05274	0.00078	0.38738	0.00963	340.2	54.19	331.3	4.75	332.5	7.05	0.327970129	
5419	0.00141	0.05114	0.00077	0.38218	0.01011	378.9	57.54	321.5	4.73	328.6	7.42	0.313172323	
5624	0.00217	0.03842	0.00064	0.29794	0.0114	461	84.2	243	3.97	264.8	8.92	0.19827369	
6066	0.00219	0.05225	0.00087	0.43716	0.01566	627.3	76.12	328.3	5.31	368.3	11.07	0.215481459	
5441	0.0012	0.04885	0.00085	0.36637	0.009	387.9	48.37	307.5	5.24	317	6.69	0.491072403	
5181	0.00244	0.05387	0.00112	0.38464	0.01808	276.9	104.35	338.2	6.87	330.4	13.26	0.216814285	
5241	0.00122	0.05413	0.00095	0.39096	0.01004	303.1	52.18	339.8	5.82	335.1	7.33	0.472189387	
5259	0.00127	0.05295	0.00094	0.38382	0.0101	311.3	53.78	332.6	5.74	329.8	7.41	0.454271666	
5879	0.0008	0.09242	0.00153	0.74883	0.01363	559.2	29.22	569.8	9.05	567.5	7.91	0.69724114	
1263	0.0015	0.05013	0.00084	0.77826	0.01392	1842.3	23.83	315.3	5.13	584.5	7.95	0.706226583	
5143	0.0014	0.0405	0.00073	0.2871	0.00834	260.1	61.4	255.9	4.54	256.3	6.58	0.408452196	
8587	0.0016	0.05963	0.00105	0.70595	0.01539	1335.2	35.71	373.4	6.41	542.3	9.16	0.570679282	
5863	0.00117	0.05188	0.0009	0.41922	0.00961	553.3	42.8	326.1	5.53	355.5	6.88	0.538389042	
5489	0.0038	0.05238	0.00145	0.39626	0.02661	407.8	147.79	329.1	8.91	338.9	19.35	0.129943084	
5297	0.00121	0.05107	0.0009	0.37283	0.00943	327.4	50.93	321.1	5.5	321.7	6.98	0.480660104	
5405	0.0014	0.0499	0.00089	0.37158	0.01028	373.1	57.1	313.9	5.44	320.8	7.61	0.418077476	
5435	0.00198	0.05819	0.00114	0.43586	0.01614	385.5	79.24	364.6	6.96	367.3	11.42	0.294889931	
5215	0.00103	0.05285	0.00091	0.37984	0.00869	292	44.59	332	5.56	326.9	6.39	0.545523584	
1209	0.00263	0.32868	0.00553	9.4667	0.16756	2897.8	20.3	1832	26.81	2384.3	16.26	0.735418102	
5441	0.00116	0.05544	0.00097	0.41574	0.01001	387.9	46.93	347.8	5.91	353	7.18	0.51193541	
0536	0.00134	0.05281	0.00095	0.3901	0.01059	354.2	55.55	331.7	5.8	334.4	7.73	0.445952579	
0528	0.00091	0.05279	0.0009	0.38412	0.00806	320.2	38.67	331.6	5.5	330.1	5.91	0.606464915	
5162	0.00198	0.04002	0.0008	0.28471	0.01108	268.5	85.62	253	4.93	254.4	8.75	0.284621146	
5628	0.00089	0.05516	0.00093	0.42783	0.00851	462.7	35.04	346.1	5.66	361.6	6.05	0.6408553	
5372	0.00102	0.05357	0.00093	0.39656	0.00891	359	42.61	336.4	5.68	339.2	6.48	0.571308376	
5345	0.00084	0.04198	0.00072	0.30927	0.00619	348	35.12	265.1	4.43	273.6	4.8	0.652204885	
5253	0.00121	0.04235	0.00075	0.3066	0.00786	308.6	51.66	267.4	4.64	271.5	6.11	0.484851227	
5467	0.00127	0.05203	0.00093	0.39203	0.01012	398.7	51.01	327	5.69	335.8	7.38	0.483541318	
5283	0.00161	0.04755	0.00089	0.34624	0.01109	321.6	67.98	299.5	5.5	301.9	8.36	0.373230014	
5055	0.00144	0.05613	0.00104	0.39098	0.0118	220.1	64.4	352	6.32	335.1	8.62	0.395816795	

h Conglomerate

$^{206}\text{Pb}/^{238}\text{U}$	$^{207}\text{Pb}/^{235}\text{U}$	Rho	Con										
1σ	1σ	1σ	1σ	1σ	1σ	Age (Ma)	1σ	Age (Ma)	1σ	Age (Ma)	1σ		
5389	0.00198	0.05301	0.00099	0.39048	0.01457	366.4	80.48	333	6.07	334.7	10.64	0.28062623	
5118	0.0019	0.05624	0.00106	0.39343	0.01483	249.1	83.27	352.7	6.46	336.9	10.81	0.28003636	
0299	0.00622	0.04668	0.00157	0.19082	0.0394	0.1	0	294.1	9.67	177.3	33.6	0.03520361	
0835	0.00152	0.05371	0.00097	0.0613	0.01114	0.1	0	337.3	5.93	60.4	10.66	0.032691	
5812	0.00212	0.04301	0.00082	0.34173	0.01265	533.8	78.5	271.5	5.06	298.5	9.57	0.28570048	
3962	0.00257	0.04061	0.00087	0.21993	0.01418	0.1	0	256.6	5.38	201.9	11.8	0.14782186	
7467	0.00487	0.05363	0.0014	0.54749	0.03459	1059.6	125.87	336.8	8.54	443.3	22.7	0.12714274	
4935	0.00202	0.04141	0.0008	0.27941	0.01152	164.5	92.83	261.6	4.95	250.2	9.14	0.24963464	
7606	0.00232	0.05706	0.00105	0.59339	0.01869	1096.7	59.75	357.7	6.4	473	11.91	0.34532237	
6911	0.0029	0.05417	0.00112	0.5119	0.02135	902.1	84.14	340.1	6.86	419.7	14.34	0.23550805	
4383	0.00341	0.05241	0.00127	0.31405	0.02406	0.1	60.33	329.3	7.79	277.3	18.59	0.10871681	
4576	0.00898	0.06471	0.00201	1.28966	0.07398	2296.8	102.23	404.2	12.15	841.1	32.81	0.12905048	
4945	0.00206	0.05433	0.00106	0.36739	0.01543	169.4	94.46	341.1	6.5	317.7	11.46	0.24966531	
5041	0.00218	0.05621	0.00112	0.38744	0.01683	213.8	97.2	352.5	6.85	332.5	12.32	0.23904237	
0511	0.00173	0.0421	0.00078	0.29415	0.01028	245.3	76.28	265.8	4.81	261.8	8.06	0.32313846	
4845	0.0027	0.05726	0.00126	0.37936	0.0209	121.2	126.12	358.9	7.71	326.6	15.38	0.17069475	
5025	0.00327	0.0545	0.0013	0.37447	0.02398	206.5	144.3	342.1	7.93	323	17.72	0.14239945	
5308	0.00331	0.05482	0.00129	0.39795	0.02445	332.1	134.99	344.1	7.89	340.2	17.76	0.15216224	
5209	0.00227	0.04139	0.00084	0.29486	0.01292	289.3	96.74	261.5	5.19	262.4	10.13	0.24332677	
5236	0.00169	0.05489	0.00101	0.39313	0.01317	301.3	71.7	344.5	6.16	336.7	9.6	0.33992598	
2751	0.02031	0.44411	0.01441	38.128	1.30373	4573	46.08	2369	64.33	3723.2	33.83	0.52927752	
6848	0.00396	0.03637	0.00066	0.83849	0.02168	2542.6	38.89	230.3	4.11	618.3	11.97	0.47462183	
6493	0.00296	0.05931	0.0013	0.52692	0.0239	772.2	93.07	371.4	7.88	429.8	15.9	0.23111683	
5331	0.00178	0.04234	0.0008	0.30882	0.01076	341.8	73.91	267.3	4.94	273.3	8.35	0.34642653	
6266	0.00478	0.05918	0.00161	0.50739	0.03784	696.7	154.7	370.6	9.81	416.7	25.49	0.11893201	
9963	0.00288	0.04177	0.0008	0.56948	0.01736	1617.2	52.87	263.8	4.93	457.7	11.23	0.3943498	
5434	0.00271	0.05599	0.00122	0.41633	0.02072	385	107.72	351.2	7.46	353.4	14.85	0.21418039	
5408	0.00214	0.05648	0.00113	0.41798	0.01691	374.3	86.22	354.2	6.9	354.6	12.11	0.29104046	
1892	0.0033	0.04731	0.00107	-0.12252	0.02133	0.1	0	298	6.6	-132.7	24.68	0.05059102	
4942	0.00501	0.05637	0.00175	0.38122	0.03779	167.7	221.11	353.5	10.69	327.9	27.78	0.08339368	
6637	0.01453	0.0564	0.00442	0.51228	0.10583	818	401.08	353.7	26.97	420	71.05	0.02753975	
9992	0.0315	0.11542	0.01264	-3.15818	0.40536	0.1	0	704.1	73.06	-NaN	-190.72	0.12952757	
0478	0.02783	0.0354	0.00596	0.23157	0.12938	88.3	996.84	224.2	37.09	211.5	106.67	0.0080949	
7655	0.02117	0.04267	0.00477	0.44712	0.11395	1109.5	471.51	269.4	29.5	375.3	79.95	0.01695669	
2957	0.04336	0.04319	0.00823	0.76596	0.21404	2092.2	494.09	272.6	50.87	577.4	123.07	0.02262872	
0657	0.00318	0.06099	0.00136	0.54849	0.02657	796.9	98.39	381.6	8.28	444	17.42	0.23196345	
1455	0.11662	0.06263	0.0153	3.55414	0.57288	3962.7	367.43	391.6	92.8	1539.4	127.73	0.08279483	
6458	0.00235	0.05273	0.00104	0.4661	0.01763	760.6	74.9	331.2	6.38	388.5	12.21	0.33212159	
5135	0.00257	0.05596	0.00121	0.39339	0.01985	256.4	111.09	351	7.41	336.8	14.46	0.23315104	
1554	0.00285	0.0793	0.00143	1.25428	0.03503	1888.3	43.68	491.9	8.57	825.3	15.78	0.49314859	
5119	0.00182	0.05119	0.00097	0.38658	0.01398	249.2	79.87	343.8	5.94	331.9	10.24	0.29388455	
4743	0.00162	0.04743	0.00068	0.2571	0.00896	70.4	79.79	248.6	4.25	232.3	7.24	0.25366247	
2596	0.00469	0.22596	0.00092	1.60583	0.03473	3023.7	32.88	324	5.65	972.5	13.53	0.30387772	
5441	0.00188	0.05441	0.00075	0.31654	0.01112	387.9	75.13	266.5	4.66	279.2	8.57	0.23773179	
7146	0.00142	0.07146	0.00063	0.38958	0.00863	970.7	40.02	250	3.93	334.1	6.3	0.44438091	
5308	0.00194	0.05308	0.00095	0.3841	0.01418	332.1	80.79	329.8	5.84	330.1	10.4	0.26290577	
0617	0.00159	0.0617	0.00089	0.45135	0.01227	663.8	54.34	333.3	5.45	378.2	8.59	0.36086395	
6749	0.00247	0.06749	0.00075	0.36795	0.01347	853	74.29	250	4.65	318.1	10	0.15269904	
4616	0.00316	0.04616	0.00112	0.34098	0.02317	5.8	157.14	336.5	6.87	297.9	17.54	0.15758954	
8367	0.00149	0.08367	0.00252	1.82753	0.03758	1284.7	34.46	948	14.04	1055.4	13.49	0.81768409	
5685	0.0019	0.05685	0.00089	0.39204	0.01331	485.1	72.69	314.6	5.49	335.9	9.71	0.2641072	
4125	0.00239	0.04125	0.00079	0.22349	0.01286	0.1	0	248.5	4.91	204.8	10.67	0.14557802	
5251	0.00136	0.05251	0.00095	0.41246	0.01129	307.8	57.73	357.2	5.77	350.6	8.12	0.40967814	
0716	0.00137	0.0716	0.00059	0.36274	0.00785	974.7	38.58	232.6	3.64	314.3	5.85	0.47697775	
4895	0.00172	0.04895	0.00092	0.35476	0.0127	145.6	80.3	330.2	5.65	308.3	9.52	0.29734651	
5072	0.00125	0.05072	0.00083	0.3554	0.00939	228.3	56.13	319.6	5.12	308.8	7.03	0.41455628	
6226	0.00192	0.06226	0.00089	0.43821	0.01388	683.2	64.42	321	5.46	369	9.8	0.28335763	
5501	0.00165	0.05501	0.00068	0.29878	0.00926	412.5	65.09	249.1	4.23	265.4	7.24	0.27887187	
6128	0.00179	0.06128	0.00069	0.33573	0.01012	649	61.48	251.2	4.28	293.9	7.69	0.26835758	
0593	0.00386	-0.00593	0.00142	-0.04542	0.02959	0.1	0	348.6	8.69	-47.2	31.47	0.18606919	
4809	0.00255	0.05732	0.00118	0.38006	0.01999	103.9	120.89	359.3	7.18	327.1	14.71	0.17479193	
6858	0.00388	0.05165	0.00121	0.48833	0.02687	886.2	112.68	324.6	7.4	403.8	18.33	0.14569534	
4673	0.00295	0.04783	0.00102	0.3081	0.01921	35	144.58	301.2	6.3	272.7	14.91	0.13427085	
4733	0.00263	0.048	0.00099	0.31315	0.01721	65.2	127.55	302.2	6.1	276.6	13.3	0.1579238	
9019	0.00177	0.03457	0.00056	0.4298	0.00941	1429.5	37.04	219.1	3.51	363	6.68	0.50273725	
4678	0.00273	0.03818	0.00073	0.24627	0.0117	38	110.3	241.6	4.56	223.5	9.53	0.1927846	

.0

sandstone

	Pb^{207}/Pb^{206}	Pb^{206}/U^{238}	Pb^{206}/U^{238}	Pb^{207}/U^{235}	Pb^{207}/U^{235}	Pb^{207}/Pb^{206}	Pb^{207}/Pb^{206}	Pb^{206}/U^{238}	Pb^{206}/U^{238}	Pb^{207}/U^{235}	Pb^{207}/U^{235}	Rho	Con
	1σ		1σ		1σ	Age (Ma)	1σ	Age (Ma)	1σ	Age (Ma)	1σ		
27	0.00183	0.0828	0.00133	0.67638	0.02101	577	65.57	512.8	7.95	524.6	12.73	0.270149	
38	0.00121	0.06812	0.00101	0.51996	0.01201	427.5	47.71	424.8	6.1	425.1	8.02	0.402909	
82	0.00357	0.04063	0.00082	0.33506	0.01962	597.2	124.15	256.8	5.1	293.4	14.92	0.116185	
13	0.002	0.05442	0.00091	0.40602	0.015	376.1	80.85	341.6	5.56	346	10.83	0.226068	
26	0.00505	0.05336	0.00125	0.46531	0.03642	717.1	160.99	335.1	7.63	387.9	25.24	0.082439	
67	0.00193	0.05311	0.00088	0.42216	0.01416	516.9	71.95	333.6	5.36	357.6	10.11	0.251548	
36	0.00283	0.04872	0.00092	0.37173	0.01876	426.3	109.78	306.6	5.63	320.9	13.88	0.152272	
74	0.00206	0.0507	0.00085	0.41746	0.0144	594.1	72.99	318.8	5.22	354.2	10.32	0.243705	
63	0.00193	0.05096	0.00085	0.41178	0.01361	553.2	70.36	320.4	5.24	350.2	9.79	0.260306	
95	0.00184	0.05533	0.00092	0.40383	0.01409	326.5	76.95	347.2	5.61	344.4	10.19	0.246751	
42	0.0027	0.05456	0.00101	0.41679	0.02013	429	105	342.4	6.19	353.8	14.42	0.168791	
91	0.00251	0.05518	0.001	0.44814	0.01895	564	90.29	346.2	6.1	376	13.29	0.196479	
35	0.00179	0.05103	0.00084	0.38228	0.01269	385.4	71.98	320.8	5.17	328.7	9.32	0.263725	
103	0.00167	0.05489	0.00089	0.40885	0.01283	372.1	67.94	344.5	5.46	348	9.25	0.287236	
76	0.00175	0.05371	0.00089	0.37588	0.01305	230	77.54	337.3	5.46	324	9.63	0.253227	
81	0.00147	0.05663	0.0009	0.40454	0.01179	277.2	63.69	355.1	5.51	344.9	8.53	0.320546	
54	0.00154	0.05042	0.00081	0.37913	0.01097	393.5	61.61	317.1	4.95	326.4	8.07	0.320564	
51	0.00303	0.04906	0.00096	0.36865	0.02025	392.1	119.78	308.7	5.88	318.7	15.03	0.144392	
29	0.00299	0.05404	0.00105	0.41192	0.022	423.6	115.78	339.3	6.44	350.3	15.82	0.147198	
64	0.00255	0.05165	0.00096	0.37494	0.01804	313.5	106.42	324.7	5.87	323.3	13.32	0.17545	
47	0.00126	0.05278	0.00077	0.39637	0.00945	390.6	50.64	331.6	4.72	339	6.87	0.353857	
62	0.00157	0.05191	0.0008	0.38377	0.01134	355.1	64.72	326.3	4.89	329.8	8.32	0.27814	
49	0.00098	0.03904	0.00054	0.32012	0.0058	584.9	35.4	246.8	3.37	282	4.46	0.495233	
47	0.00141	0.04828	0.00072	0.35586	0.00956	348.6	58.58	303.9	4.45	309.1	7.16	0.310418	
73	0.00184	0.03908	0.00062	0.28411	0.00991	317.3	77.45	247.1	3.86	253.9	7.83	0.22654	
74	0.00162	0.05078	0.00079	0.3762	0.01142	360	66.44	319.3	4.82	324.2	8.42	0.269765	
12	0.00264	0.05365	0.00095	0.4225	0.01931	495.6	99.11	336.9	5.81	357.8	13.79	0.164507	
19	0.00179	0.0494	0.00079	0.35547	0.01216	293.7	76.14	310.9	4.83	308.8	9.11	0.228138	
12	0.00162	0.05093	0.00079	0.35952	0.01141	250	70.99	320.2	4.85	311.9	8.52	0.250566	
52	0.00146	0.04759	0.00072	0.34116	0.00975	285.5	63.1	299.7	4.43	298	7.38	0.297584	
23	0.00375	0.0474	0.00095	0.40664	0.02406	682	123.88	298.5	5.86	346.5	17.37	0.114354	
98	0.00157	0.04865	0.00075	0.34194	0.01058	240.1	69.27	306.2	4.61	298.6	8	0.258487	
47	0.00278	0.05267	0.00095	0.3956	0.0199	390.7	109.98	330.9	5.81	338.5	14.48	0.138293	
33	0.00285	0.05369	0.00097	0.42438	0.02078	503.7	106.19	337.2	5.96	359.2	14.81	0.142841	
76	0.0012	0.05127	0.00075	0.37296	0.00879	318.5	50.73	322.3	4.57	321.8	6.5	0.365667	
22	0.00131	0.0488	0.00072	0.35121	0.00905	294.4	56.34	307.1	4.44	305.6	6.8	0.331257	
35	0.00218	0.05549	0.00093	0.38518	0.01653	211	97.21	348.2	5.71	330.8	12.12	0.172378	
32	0.002	0.05079	0.00083	0.35236	0.01396	210	89.75	319.3	5.11	306.5	10.48	0.198452	
11	0.00145	0.05092	0.00077	0.35184	0.01034	200.3	66.01	320.2	4.74	306.1	7.77	0.286937	
59	0.00199	0.0553	0.0009	0.42615	0.01511	447.9	77.18	347	5.48	360.4	10.76	0.220741	
45	0.00206	0.05132	0.00084	0.38523	0.01448	389.5	81.95	322.6	5.17	330.9	10.61	0.202715	
88	0.00135	0.06595	0.00098	0.48986	0.01259	365.8	55.54	411.7	5.93	404.8	8.58	0.331983	
101	0.00292	0.04774	0.00088	0.35552	0.01896	371.4	116.92	300.6	5.43	308.9	14.2	0.132742	
67	0.00114	0.04965	0.00071	0.36734	0.00816	357	47.28	312.3	4.39	317.7	6.06	0.388415	
48	0.00237	0.05209	0.00088	0.44156	0.01682	656.1	80.51	327.3	5.41	371.3	11.85	0.194541	
53	0.00184	0.04797	0.00075	0.4319	0.01228	783.9	58.25	302.1	4.6	364.5	8.7	0.291174	
14	0.0015	0.04962	0.00075	0.3704	0.0104	376.8	60.94	312.2	4.62	319.9	7.7	0.293597	
21	0.0013	0.05117	0.00075	0.37541	0.00942	337.9	54.39	321.7	4.63	323.7	6.96	0.336567	
84	0.00229	0.04438	0.0007	0.54362	0.01406	1400.7	48.52	279.9	4.31	440.8	9.25	0.310429	
86	0.0013	0.05294	0.00078	0.41506	0.00981	485.6	49.77	332.5	4.75	352.5	7.04	0.363229	
77	0.0017	0.05037	0.00077	0.42902	0.01194	666.2	57.91	316.8	4.76	362.5	8.48	0.294767	
82	0.00228	0.03782	0.0006	0.43711	0.01187	1288.3	52.03	239.3	3.73	368.2	8.38	0.289234	
85	0.00256	0.03782	0.00067	0.25995	0.01323	188.1	115.48	239.3	4.14	234.6	10.66	0.147978	
09	0.00255	0.04755	0.00084	0.33368	0.01651	236.3	111.43	299.4	5.17	292.4	12.57	0.143219	
32	0.00142	0.05304	0.00078	0.44109	0.01069	615	50.06	333.2	4.8	371	7.53	0.349933	
85	0.00156	0.05126	0.00078	0.40884	0.01119	523.8	58.32	322.2	4.78	348	8.06	0.30432	
65	0.00387	0.59603	0.00829	23.39248	0.36794	3388.6	21.04	3013.8	33.5	3243.4	15.32	0.585116	
67	0.00128	0.0547	0.0008	0.40478	0.00998	357.3	53.21	343.3	4.92	345.1	7.21	0.350797	
22	0.00258	0.05379	0.00094	0.42442	0.01893	499.6	97	337.8	5.78	359.2	13.5	0.167878	
74	0.0016	0.04972	0.00077	0.35471	0.01107	274.1	69.46	312.8	4.73	308.3	8.3	0.266419	
55	0.00235	0.05438	0.00093	0.41615	0.01747	432	91.89	341.4	5.7	353.3	12.53	0.182415	
28	0.00345	0.04595	0.00071	1.07263	0.02217	2550.6	33.74	289.6	4.39	740	10.86	0.392323	
78	0.00126	0.0395	0.00058	0.28202	0.00703	275.5	54.57	249.8	3.6	252.3	5.57	0.334471	
54	0.00117	0.10655	0.0015	0.97753	0.01858	823.4	36.26	652.7	8.75	692.3	9.54	0.467674	

sandstone Member

²⁰⁶ Pb/ ²⁰⁷ Pb	²⁰⁶ Pb/ ²³⁸ U	²⁰⁶ Pb/ ²³⁸ U	²⁰⁷ Pb/ ²³⁵ U	²⁰⁷ Pb/ ²³⁵ U	²⁰⁷ Pb/ ²³⁵ U	²⁰⁷ Pb/ ²⁰⁶ Pb	²⁰⁷ Pb/ ²⁰⁶ Pb	²⁰⁶ Pb/ ²³⁸ U	²⁰⁶ Pb/ ²³⁸ U	²⁰⁷ Pb/ ²³⁵ U	²⁰⁷ Pb/ ²³⁵ U	Rho	Con
1σ		1σ		1σ	Age (Ma)	1σ	Age (Ma)	1σ	Age (Ma)	1σ	Age (Ma)		
211	0.00177	0.0538	0.00097	0.38644	0.0134	290.2	75.79	337.8	5.91	331.8	9.82	0.298894	
222	0.00254	0.05423	0.00111	0.39022	0.01883	294	107.55	340.5	6.79	334.5	13.75	0.192257	
507	0.00163	0.05236	0.00092	0.36593	0.01206	227	72.47	329	5.64	316.6	8.96	0.311947	
559	0.00265	0.05188	0.00107	0.39755	0.01873	435.8	102.41	326	6.56	339.9	13.61	0.191721	
274	0.00169	0.0524	0.00093	0.38096	0.01255	317.7	71.38	329.2	5.68	327.7	9.23	0.319343	
157	0.00244	0.04257	0.00082	0.37894	0.01433	760.5	77.82	268.7	5.07	326.3	10.55	0.256116	
358	0.00364	0.0564	0.00092	1.69942	0.03288	2970.3	26.61	353.7	5.64	1008.3	12.37	0.575249	
376	0.00177	0.05418	0.00097	0.40152	0.01352	360.9	72.47	340.1	5.92	342.7	9.8	0.307161	
795	0.00355	0.05347	0.00135	0.3534	0.02554	95.5	167.47	335.8	8.28	307.3	19.16	0.103874	
205	0.00204	0.04218	0.0008	0.30261	0.01192	287.4	87.06	266.3	4.92	268.4	9.29	0.251137	
771	0.00235	0.03939	0.00078	0.27533	0.01267	227.5	103.49	249	4.85	246.9	10.09	0.198715	
118	0.00209	0.0538	0.00103	0.37218	0.01553	203.4	93.88	337.8	6.3	321.3	11.49	0.233428	
267	0.00148	0.05314	0.00091	0.38588	0.01138	314.7	62.75	333.8	5.56	331.4	8.34	0.369678	
309	0.0034	0.04983	0.00122	0.27542	0.02301	0.1	0	313.5	7.48	247	18.32	0.094507	
353	0.00208	0.05268	0.001	0.36696	0.01515	219.5	92.42	331	6.1	317.4	11.25	0.236286	
391	0.00189	0.05928	0.00108	0.41604	0.01562	236.7	83.24	371.3	6.6	353.2	11.2	0.265559	
394	0.00235	0.04289	0.00087	0.23615	0.01382	0.1	0	270.7	5.39	215.3	11.35	0.157679	
578	0.00139	0.0392	0.00065	0.30143	0.00802	443.4	54.17	247.9	4.06	267.5	6.25	0.410133	
514	0.00313	0.04645	0.00104	0.32909	0.01969	258.7	133.98	292.7	6.39	288.9	15.04	0.139194	
332	0.00325	0.06002	0.00142	0.27471	0.0267	0.1	0	375.7	8.63	246.5	21.26	0.092094	
371	0.00253	0.04995	0.00103	0.34228	0.01729	181.4	114.55	314.2	6.31	298.9	13.08	0.185561	
326	0.00276	0.05304	0.00115	0.36746	0.01989	207	122.54	333.2	7.03	317.8	14.77	0.163761	
246	0.00223	0.05481	0.00106	0.39639	0.01686	305.6	94.45	344	6.49	339	12.26	0.22865	
252	0.00124	0.04048	0.00067	0.29307	0.00748	308.3	52.61	255.8	4.14	261	5.87	0.435486	
158	0.00182	0.05264	0.00095	0.39606	0.0135	394.9	72.43	330.7	5.82	338.8	9.82	0.3053	
297	0.00313	0.05348	0.0012	0.39046	0.02269	327.3	128.61	335.8	7.37	334.7	16.57	0.149061	
397	0.0023	0.05723	0.00114	0.38628	0.01806	146.2	106.47	358.7	6.95	331.6	13.23	0.202266	
511	0.00507	0.06384	0.00197	0.40571	0.04362	3.1	245.4	398.9	11.94	345.8	31.51	0.063564	
336	0.00315	0.0578	0.00132	0.40127	0.02471	211.7	138.85	362.2	8.03	342.6	17.9	0.142614	
398	0.00266	0.05324	0.00109	0.39614	0.01936	369.9	106.75	334.4	6.7	338.8	14.08	0.189552	
707	0.00195	0.05737	0.00107	0.37225	0.01557	52.3	96.5	359.6	6.54	321.3	11.52	0.244249	
346	0.00239	0.05163	0.00102	0.38049	0.01699	348.2	97.94	324.6	6.26	327.4	12.5	0.218513	
124	0.00211	0.05279	0.00101	0.37282	0.0154	251.6	91.95	331.6	6.18	321.7	11.39	0.238271	
161	0.00175	0.04199	0.00076	0.29872	0.01038	268	76.1	265.2	4.68	265.4	8.11	0.306293	
369	0.00313	0.0434	0.001	0.29131	0.01841	133.2	144.57	273.9	6.16	259.6	14.48	0.134718	
254	0.00192	0.05741	0.00106	0.41578	0.01542	309	81.15	359.8	6.46	353	11.06	0.278136	
367	0.00259	0.04494	0.00096	0.22735	0.01594	0.1	0	283.4	5.92	208	13.19	0.130734	
505	0.0032	0.05299	0.00118	0.32902	0.02313	0.1	111.26	332.8	7.23	288.8	17.67	0.125316	
763	0.00314	0.06298	0.00146	0.41354	0.02679	80.2	150.06	393.7	8.83	351.4	19.24	0.129195	
503	0.00211	0.08886	0.00167	0.68636	0.02617	453.4	81.41	548.8	9.91	530.6	15.76	0.271319	
243	0.00166	0.05296	0.00094	0.38271	0.01249	304.1	70.29	332.7	5.73	329	9.17	0.326009	
534	0.00229	0.0516	0.00101	0.3225	0.01628	0.1	80.02	324.3	6.21	283.8	12.5	0.192511	
142	0.00207	0.0523	0.00098	0.3923	0.01505	388.2	82.36	328.6	6.02	336	10.97	0.261542	
361	0.00222	0.05022	0.00099	0.34344	0.01538	176.7	101.24	315.9	6.05	299.8	11.62	0.221783	
541	0.00244	0.06343	0.00131	0.40577	0.02124	18.8	121.93	396.5	7.93	345.8	15.34	0.186116	
375	0.00244	0.04209	0.00085	0.28863	0.01407	183.3	110.37	265.8	5.28	257.5	11.09	0.192351	
385	0.00138	0.04876	0.00082	0.36195	0.00992	364.5	56.77	306.9	5.06	313.7	7.4	0.409229	
363	0.00134	0.05367	0.0009	0.39679	0.01066	355.5	55.54	337	5.52	339.3	7.75	0.420258	
501	0.00214	0.0416	0.00081	0.25808	0.01231	0.1	56.5	262.7	5	233.1	9.93	0.211973	
398	0.00365	0.03779	0.00085	-0.36974	0.01859	0.1	0	239.1	5.28	-468.7	29.95	-0.17223	
141	0.00491	0.07527	0.00128	2.74346	0.05736	3273.2	28.92	467.9	7.69	1340.3	15.56	0.536487	
223	0.00206	0.04168	0.00079	0.30007	0.01192	295.7	87.55	263.2	4.91	266.5	9.31	0.253454	
711	0.00232	-0.03273	0.00065	-0.03206	0.01047	0.1	0	-214.5	4.31	-33.1	10.98	0.044206	
357	0.0021	0.05633	0.00109	0.37714	0.01633	127.4	98.5	353.2	6.65	324.9	12.04	0.2267	
145	0.00174	0.06741	0.00123	0.38513	0.0164	0.1	0	420.5	7.46	330.8	12.02	0.247154	
193	0.00285	0.0568	0.00125	0.32827	0.02206	0.1	0	356.1	7.65	288.2	16.87	0.128568	
199	0.0019	0.05465	0.00102	0.3389	0.01444	0.1	43.06	343	6.23	296.3	10.95	0.239121	
327	0.0018	0.04168	0.00076	0.28883	0.01055	207.6	81.15	263.2	4.73	257.6	8.31	0.2887	
185	0.00232	0.04473	0.00089	0.3197	0.01428	278.9	99.12	282.1	5.47	281.7	10.99	0.218826	
386	0.00262	0.05688	0.00116	0.44583	0.02047	485.4	99.44	356.7	7.07	374.4	14.38	0.214043	
378	0.00226	0.04647	0.00094	0.29962	0.01446	37.9	112.09	292.8	5.76	266.1	11.3	0.207091	
386	0.00308	0.12377	0.003	0.15111	0.05246	0.1	0	751.9	17.21	142.9	46.27	0.015714	

.4

High Sandstone

²⁰⁶ Pb/ ²⁰⁷ Pb 1σ	²⁰⁶ Pb/ ²³⁸ U 1σ	²⁰⁶ Pb/ ²³⁸ U 1σ	²⁰⁷ Pb/ ²³⁵ U 1σ	²⁰⁷ Pb/ ²³⁵ U 1σ	²⁰⁷ Pb/ ²³⁵ U Age (Ma)	²⁰⁷ Pb/ ²⁰⁶ Pb 1σ	²⁰⁷ Pb/ ²⁰⁶ Pb Age (Ma)	²⁰⁶ Pb/ ²³⁸ U 1σ	²⁰⁶ Pb/ ²³⁸ U Age (Ma)	²⁰⁷ Pb/ ²³⁵ U 1σ	²⁰⁷ Pb/ ²³⁵ U Age (Ma)	Rho	Co
96	0.00189	0.0426	0.00085	0.31109	0.01136	327	78.97	268.9	5.24	275	8.8	0.314302	
51	0.00193	0.05233	0.00104	0.40053	0.01432	432.4	75.66	328.8	6.38	342	10.38	0.326773	
17	0.00428	0.05658	0.00161	0.48135	0.03226	663.7	142.01	354.8	9.81	399	22.11	0.128327	
47	0.00176	0.0519	0.00101	0.3898	0.0131	390.3	70.27	326.2	6.18	334.2	9.57	0.354824	
79	0.00134	0.04981	0.00091	0.37629	0.01011	403.8	53.43	313.3	5.57	324.3	7.46	0.466016	
52	0.00187	0.05327	0.00105	0.40784	0.01419	433.1	73.3	334.6	6.43	347.3	10.24	0.338749	
97	0.00178	0.05177	0.00101	0.37809	0.01314	327.3	74.56	325.4	6.21	325.6	9.68	0.338637	
09	0.00158	0.05186	0.00098	0.40106	0.01204	455.5	61.44	325.9	5.98	342.4	8.72	0.40969	
89	0.00139	0.04039	0.00074	0.30009	0.00839	366.2	56.91	255.2	4.6	266.5	6.55	0.441248	
14	0.0018	0.06653	0.0013	0.50585	0.01713	417.9	70.78	415.2	7.86	415.7	11.55	0.349802	
23	0.00157	0.03904	0.00074	0.28653	0.00892	338.6	65.36	246.9	4.58	255.8	7.04	0.388503	
89	0.00266	0.05495	0.00125	0.4083	0.01994	366.4	106.79	344.8	7.61	347.7	14.38	0.209777	
47	0.00171	0.03945	0.00077	0.27994	0.00964	261.8	74.5	249.4	4.76	250.6	7.65	0.344439	
29	0.00255	0.04914	0.00108	0.3814	0.01723	463.2	98.26	309.2	6.66	328.1	12.66	0.237535	
51	0.00235	0.05199	0.00112	0.39075	0.01686	392.2	93.17	326.7	6.83	334.9	12.31	0.251328	
29	0.00198	0.05396	0.00108	0.42626	0.01516	502.2	74.93	338.8	6.59	360.5	10.79	0.330844	
08	0.0017	0.05366	0.00103	0.40754	0.01315	415.3	66.78	337	6.31	347.1	9.49	0.368923	
77	0.00214	0.05494	0.00114	0.40739	0.01638	361.4	87.05	344.8	6.98	347	11.81	0.277602	
94	0.00213	0.05552	0.00114	0.43589	0.0166	488.5	81.24	348.3	6.96	367.3	11.74	0.302176	
72	0.00157	0.05105	0.00096	0.39222	0.01179	440.9	61.4	321	5.9	336	8.6	0.409796	
95	0.00192	0.03949	0.00079	0.29921	0.01072	410.3	75.51	249.6	4.89	265.8	8.38	0.322966	
37	0.00128	0.04921	0.0009	0.3689	0.00965	386.2	51.61	309.7	5.5	318.8	7.16	0.485482	
73	0.00231	0.05693	0.00121	0.44529	0.01823	480.2	88.05	356.9	7.36	374	12.81	0.269922	
14	0.0024	0.06223	0.00132	0.51604	0.02073	608.5	83.95	389.2	8.03	422.5	13.88	0.27644	
57	0.00193	0.0338	0.00062	0.41746	0.01015	1416.2	40.61	214.3	3.88	354.2	7.27	0.519449	
28	0.00179	0.05164	0.00101	0.40075	0.01332	462.7	69.44	324.6	6.19	342.2	9.65	0.365881	
58	0.00449	0.0497	0.00149	0.40151	0.02973	551.7	159.18	312.7	9.15	342.7	21.54	0.114131	
44	0.00174	0.04973	0.00097	0.37299	0.01243	387.6	69.88	312.8	5.95	321.9	9.19	0.359968	
77	0.00193	0.03989	0.0008	0.29579	0.01088	361.4	78.83	252.2	4.98	263.1	8.53	0.316419	
92	0.00247	0.04977	0.00107	0.41121	0.01702	600.7	86.88	313.1	6.58	349.7	12.25	0.267529	
49	0.0027	0.05601	0.00126	0.45177	0.02074	548.2	97.86	351.3	7.7	378.5	14.51	0.233714	
53	0.00189	0.05015	0.00101	0.36647	0.01343	328.6	79.02	315.4	6.19	317	9.98	0.323105	
47	0.00255	0.03751	0.00084	0.28293	0.01313	400.1	100.7	237.4	5.19	253	10.39	0.231848	
07	0.00192	0.04887	0.00096	0.40897	0.01345	628.5	66.6	307.6	5.91	348.1	9.69	0.361397	
43	0.00182	0.06175	0.00122	0.46346	0.01604	389	72.57	386.2	7.42	386.7	11.13	0.343737	
46	0.00166	0.05257	0.00101	0.41656	0.01276	509	62.56	330.3	6.16	353.6	9.14	0.401704	
58	0.00232	0.05338	0.00113	0.4269	0.01724	529.3	85.8	335.2	6.93	361	12.27	0.280156	
93	0.00128	0.03859	0.0007	0.29761	0.00765	449.1	49.78	244.1	4.36	264.5	5.99	0.499729	
68	0.00205	0.0389	0.00081	0.27188	0.01113	226.4	90.85	246	5.03	244.2	8.89	0.277587	
75	0.00229	0.05491	0.00116	0.44482	0.01754	557.8	82.83	344.6	7.07	373.6	12.33	0.289193	
18	0.00227	0.05109	0.00111	0.36053	0.01607	249	99.07	321.2	6.79	312.6	11.99	0.253816	
27	0.00196	0.06267	0.00129	0.44304	0.01727	252.9	85.56	391.8	7.82	372.4	12.15	0.300195	
19	0.00212	0.05327	0.00111	0.40533	0.0158	419.6	83.07	334.5	6.78	345.5	11.42	0.294329	
09	0.00369	0.05219	0.00129	0.52605	0.0259	1016.6	98.9	328	7.9	429.2	17.23	0.199767	
96	0.00157	0.04774	0.00092	0.34206	0.0109	283.8	67.41	300.6	5.66	298.7	8.25	0.385793	
18	0.00181	0.04083	0.00082	0.29162	0.01052	276.5	78.06	258	5.06	259.8	8.27	0.333853	
24	0.00213	0.05159	0.00109	0.37274	0.01532	302.9	89.96	324.3	6.67	321.7	11.33	0.278311	
32	0.00271	0.05771	0.00133	0.44025	0.02142	425.1	105.65	361.7	8.11	370.4	15.1	0.222316	
54	0.00268	0.05488	0.00127	0.40511	0.0201	351.6	108.54	344.4	7.73	345.4	14.52	0.214112	
77	0.00161	0.04954	0.00096	0.36046	0.01163	319	67.99	311.7	5.9	312.6	8.68	0.388386	
47	0.00225	0.05469	0.00118	0.38814	0.01706	262.1	97.32	343.2	7.23	333	12.48	0.256465	
43	0.00197	0.05107	0.00105	0.36214	0.01415	260.1	85.64	321.1	6.47	313.8	10.55	0.30012	
92	0.00166	0.05497	0.00106	0.44659	0.01348	564.1	60.35	345	6.45	374.9	9.46	0.420214	
91	0.00256	0.05474	0.00119	0.4673	0.01938	670.9	85.95	343.6	7.29	389.3	13.41	0.267693	
55	0.0027	0.05258	0.00121	0.40236	0.01944	432.2	104.65	330.3	7.4	343.4	14.08	0.2236	
92	0.00189	0.05086	0.00103	0.37116	0.01363	325.5	79.1	319.8	6.32	320.5	10.1	0.324849	
68	0.00413	0.05612	0.00163	0.43085	0.031	439.2	157.5	352	9.98	363.8	22	0.124118	
99	0.00205	0.05185	0.00108	0.38602	0.01496	370.4	83.18	325.9	6.59	331.5	10.96	0.306015	
19	0.00195	0.04113	0.00081	0.37543	0.01168	812.5	60.37	259.9	4.99	323.7	8.62	0.398085	
48	0.00272	0.05267	0.00123	0.38109	0.01955	306.3	113.7	330.9	7.55	327.8	14.37	0.204839	